Neutron Skin of ^{208}Pb from Coherent Pion Photoproduction

C.M. Tarbert et al., Phys. Rev. Lett. **112**, 242502 (2014)

Crystal Ball

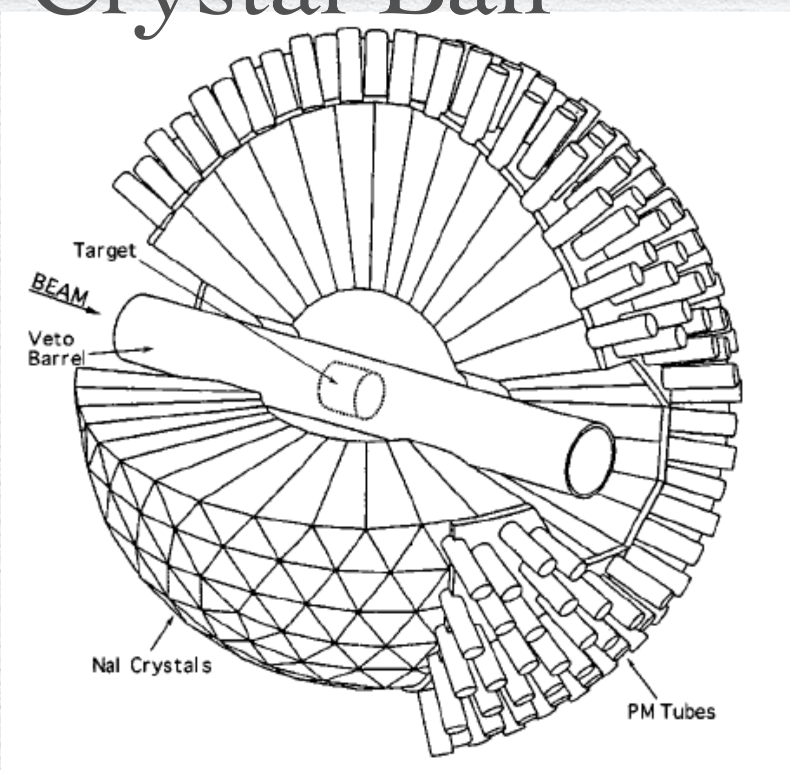

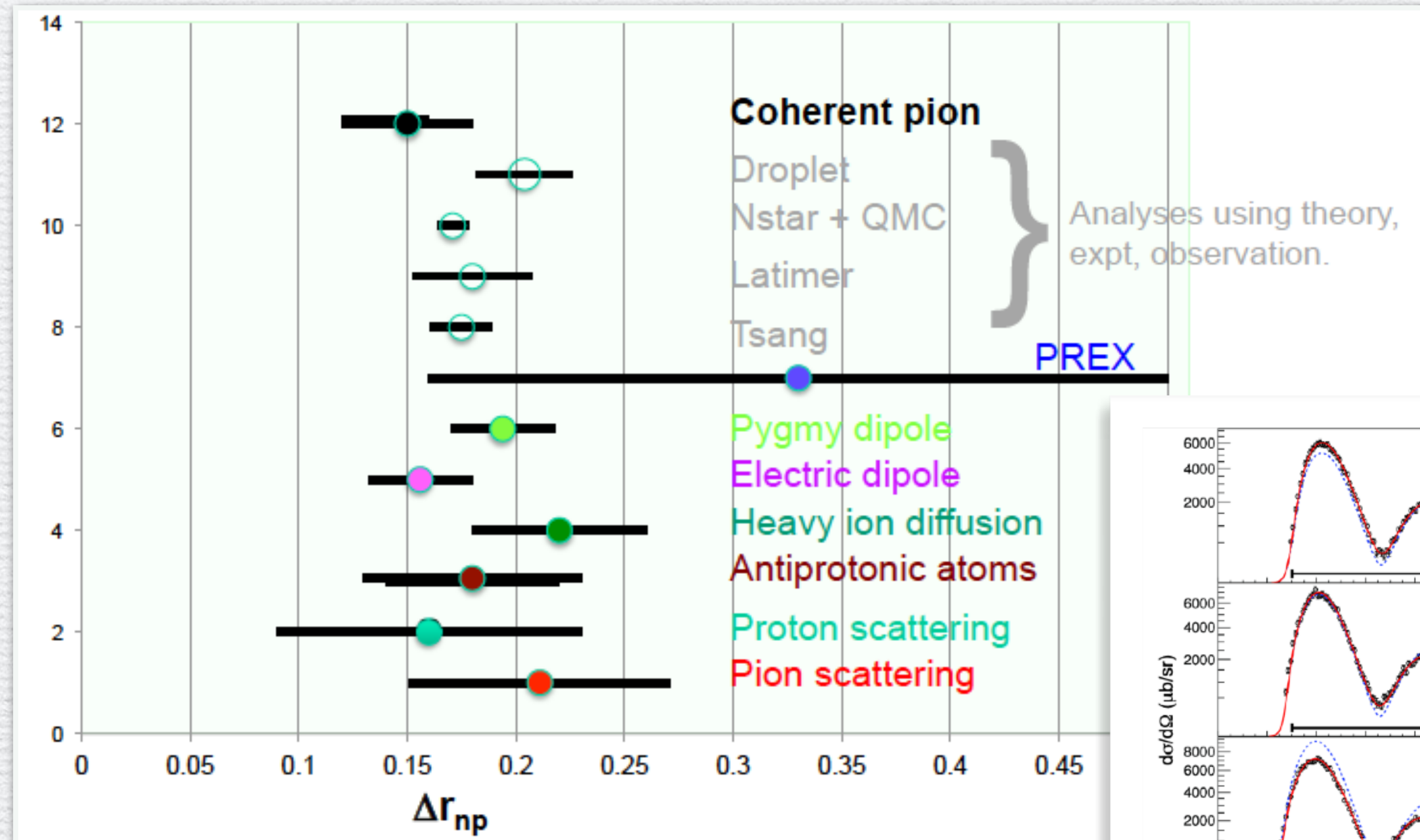

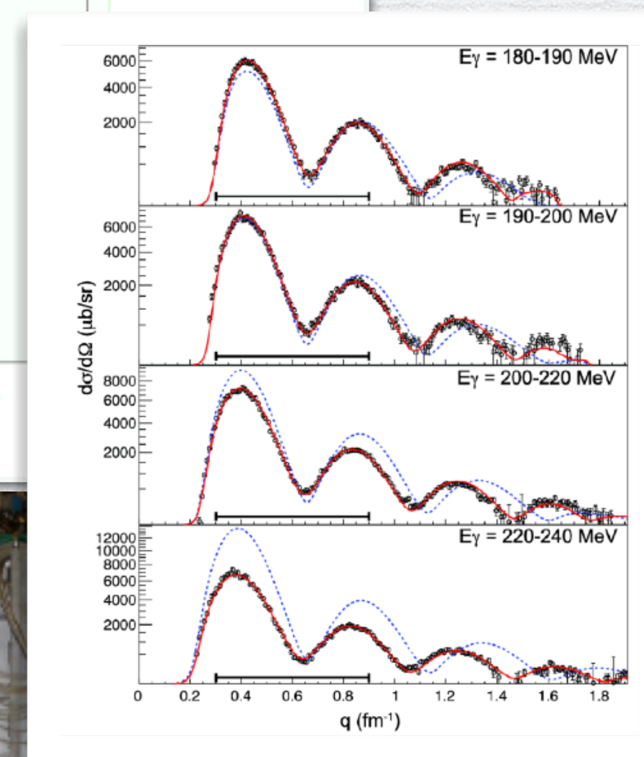

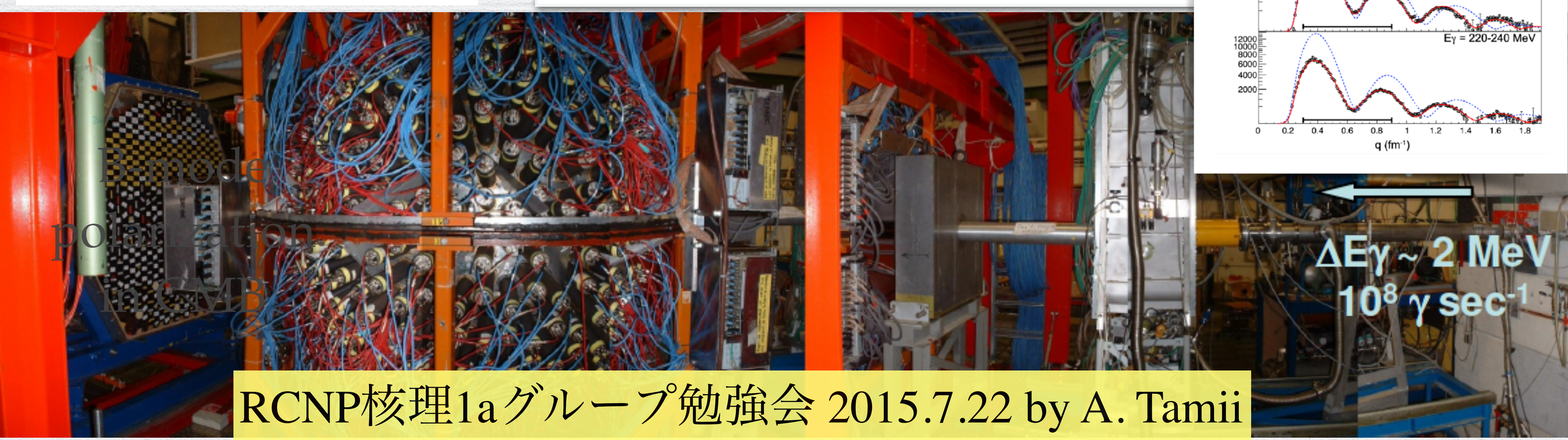

Neutron Skins of Nuclei: from laboratory to stars
Introductory Workshop
May 4-7, 2015 at MITP, Mainz

	4 May	5 May	6 May	7 May
9:00-10:30	Welcome and Introduction – **Chuck**	Pygmy (45) **Aumann** *Discussion*	**Schwenk** (45) + *Discussion*	Wrap-up – **Jorge**
10:30-11:00	Coffee Break	Coffee Break	Coffee Break	Coffee Break
11:00-12:30	PREX (45)- **Kumar** *Discussion*	p-scattering (45) – **Egelhof** *Discussion*	**Hagen** (45) + *Discussion*	*Discussion and homework assignements*
12:30-14:00	Lunch	Lunch	Lunch	Lunch
14:00-15:30	EDP (45) – **Tamii** *Discussion*	**Gandolfi** (45) + *Discussion*	**Li** (45) + *Discussion*	
15:30-16:00	Coffee Break	Coffee Break	Coffee Break	
16:00 – 17:30	Pi0 (45) – **Watts** *Discussion*	*Chuck Colloquium*	**Roca-Maza** (45) + *Discussion*	
17:30-18:30	*Contingency*		*Contingency*	

Organized by
Concettina Sfienti

Neutron Skins of Nuclei: from laboratory to stars
Introductory Workshop
May 4-7, 2015 at MITP, Mainz



	4 May	5 May	6 May	7 May
9:00-10:30	Welcome and Introduction – **Chuck**	Pygmy (45) **Aumann** *Discussion* PDR	**Schwenk** (45) + *Discussion*	Wrap-up – **Jorge**
10:30-11:00	Coffee Break	Coffee Break	Coffee Break	Coffee Break
11:00-12:30	PREX (45)- **Kumar** *Discussion* PREX	p-scattering (45) – **Egelhof** *Discussion* p-elastic	**Hagen** (45) + *Discussion*	*Discussion and homework assignements*
12:30-14:00	Lunch	Lunch	Lunch	Lunch
14:00-15:30	EDP (45) – **Tamii** *Discussion* DP	**Gandolfi** (45) + *Discussion*	**Li** (45) + *Discussion*	
15:30-16:00	Coffee Break	Coffee Break	Coffee Break	
16:00 – 17:30	Pi0 (45) – **Watts** *Discussion* Coher. π	*Chuck Colloquium*	**Roca-Maza** (45) + *Discussion*	
17:30-18:30	*Contingency*		*Contingency*	


Big-debates were held for each of the experiments!

MITP Conference on Neutron Skin, 17-27 May, 2015

Two Approaches for the Neutron Skin Thickness

Probing the matter/neutron/weak-charge distribution

Takes the difference from the charge (or p) distribution → ΔR_{np}

- Less / no model dependence
- Data must be highly accurate

$$\frac{\sigma\left(\Delta R_{np}\right)}{R_p} \sim \frac{0.02\ fm}{5.45\ fm} \sim 4\times 10^{-3}$$

PREX

p elastic scattering

coherent π production

Probing the difference between the p/n distribution

- Requires theoretical models
- Data can be less accurate

$$\frac{\sigma\left(\Delta R_{np}\right)}{\Delta R_{np}} \sim \frac{0.02\ fm}{0.2\ fm} \sim 10^{-1}$$

Dipole Polarizability

PDR

GDR

Constraints on *J* and *L*

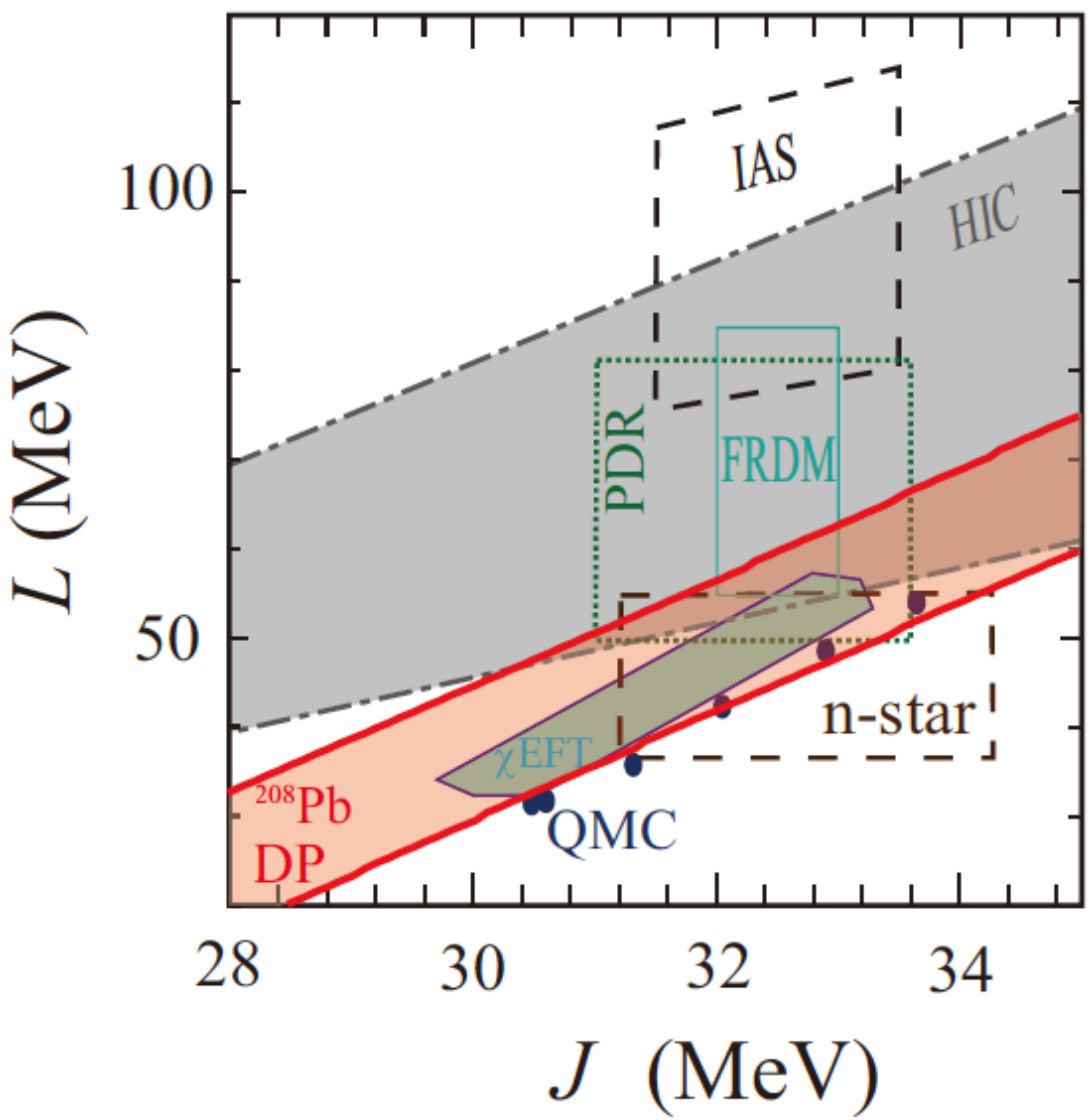

AT et al., EPJA**50**, 28 (2014).

M.B. Tsang *et al*., PRC**86**, 015803 (2012)

C.J. Horowitz et al., JPG41, 093001 (2014)

DP: Dipole Polarizability
HIC: Heavy Ion Collision
PDR: Pygmy Dipole Resonance
IAS: Isobaric Analogue State
FRDM: Finite Range Droplet Model (nuclear mass analysis)
n-star: Neutron Star Observation
cEFT: Chiral Effective Field Theory

QMC: S. Gandolfi, EPJA50, 10(2014).

I. Tews et al., PRL110, 032504 (2013)

PRL 112, 242502 (2014) PHYSICAL REVIEW LETTERS week ending 20 JUNE 2014

Neutron Skin of ^{208}Pb from Coherent Pion Photoproduction

C. M. Tarbert,[1] D. P. Watts,[1,*] D. I. Glazier,[1] P. Aguar,[2] J. Ahrens,[2] J. R. M. Annand,[3] H. J. Arends,[2] R. Beck,[2,4] V. Bekrenev,[5] B. Boillat,[6] A. Braghieri,[7] D. Branford,[1] W. J. Briscoe,[8] J. Brudvik,[9] S. Cherepnya,[10] R. Codling,[3] E. J. Downie,[3] K. Foehl,[1] P. Grabmayr,[11] R. Gregor,[12] E. Heid,[2] D. Hornidge,[13] O. Jahn,[2] V. L. Kashevarov,[10] A. Knezevic,[14] R. Kondratiev,[15] M. Korolija,[14] M. Kotulla,[6] D. Krambrich,[2,4] B. Krusche,[6] M. Lang,[2,4] V. Lisin,[15] K. Livingston,[3] S. Lugert,[12] I. J. D. MacGregor,[3] D. M. Manley,[16] M. Martinez,[2] J. C. McGeorge,[3] D. Mekterovic,[14] V. Metag,[12] B. M. K. Nefkens,[9] A. Nikolaev,[2,4] R. Novotny,[12] R. O. Owens,[3] P. Pedroni,[7] A. Polonski,[15] S. N. Prakhov,[9] J. W. Price,[9] G. Rosner,[3] M. Rost,[2] T. Rostomyan,[7] S. Schadmand,[12] S. Schumann,[2,4] D. Sober,[17] A. Starostin,[9] I. Supek,[14] A. Thomas,[2] M. Unverzagt,[2,4] Th. Walcher,[2] L. Zana,[1] and F. Zehr[6]
(Crystal Ball at MAMI and A2 Collaboration)

Abstract

Information on the size and shape of the neutron skin on ^{208}Pb is extracted from coherent pion photoproduction cross sections measured using the Crystal Ball detector together with the Glasgow tagger at the MAMI electron beam facility. On exploitation of an interpolated fit of a theoretical model to the measured cross sections, the half-height radius and diffuseness of the neutron distribution are found to be $c_n = 6.70 \pm 0.03(\text{stat.})$ fm and $a_n = 0.55 \pm 0.01(\text{stat.})^{+0.02}_{-0.03}(\text{sys.})$ fm, respectively, corresponding to a neutron skin thickness $\Delta r_{np} = 0.15 \pm 0.03(\text{stat.})^{+0.01}_{-0.03}(\text{sys.})$ fm. The results give the first successful extraction of a neutron skin thickness with an electromagnetic probe and indicate that the skin of ^{208}Pb has a halo character. The measurement provides valuable new constraints on both the structure of nuclei and the equation of state for neutron-rich matter.

Structure of the Paper

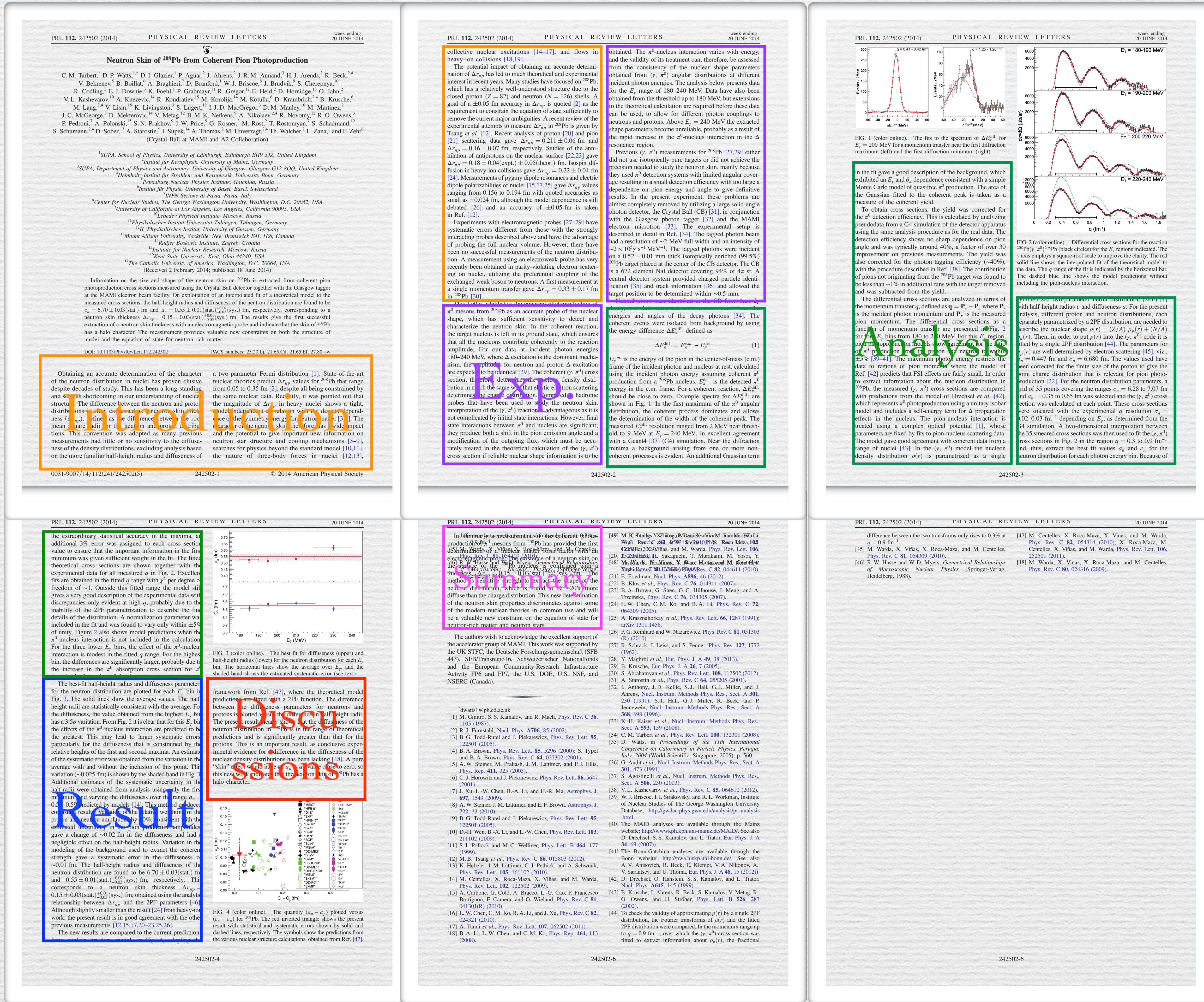

Introductions: Neutron Skin Thickness

Neutron distribution in nuclei

Neutron skin thickness (Δr_{np})

$$\Delta r_{np} \equiv \sqrt{\left\langle r^2 \right\rangle_n} - \sqrt{\left\langle r^2 \right\rangle_p}$$

difference of the root mean square radii of *n* and *p*

➡ no sensitivity to the diffuseness of the density distributions

Predictions of "state of the art" nuclear theories

$$\Delta r_{np} = 0.05 - 0.35 \text{ fm}$$

➡ **density dependence of the symmetry energy**

- Neutron star structure/cooling mechanism [5-9]
- Physics beyond the standard model [10,11]
- Three-body forces in nuclei [12,13]
- Collective nuclear excitations [14-17]
- Flows in heavy-ion collision [18-19]

Introductions: Neutron Skin Thickness

Neutron distribution in nuclei

two parameter Fermi (2PF) distribution

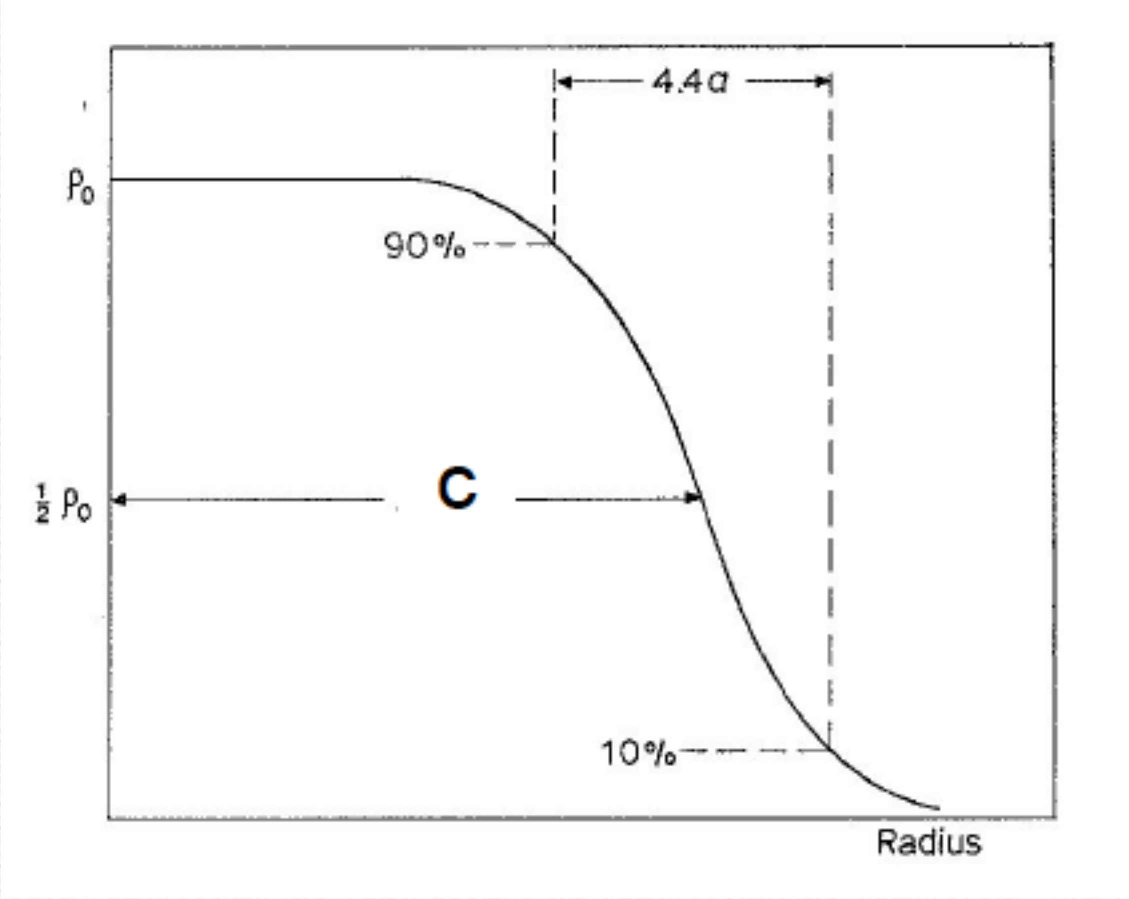

$$\rho(r) = \frac{\rho_0}{1 + \exp\left(\frac{r-c}{a}\right)}$$

Introductions: The case of ^{208}Pb

A goal of 0.05 fm accuracy is quoted [2] [2] R. J. Furnstahl, NPA706, 85 (2002).

to constrain the EoS sufficiently to remove the current major ambiguities

Taken from [12] M. B. Tsang et al., PRC86, 015803 (2012).

proton scattering	$\Delta r_{np} = 0.211 \pm 0.06$ fm	[20]
pion scattering	$\Delta r_{np} = 0.16 \pm 0.07$ fm	[21]
anti-proton annihilation	$\Delta r_{np} = 0.18 \pm 0.04_{exp.} \pm 0.05_{theor.}$ fm	[22,23]
Isospin-diffusion heavy ion collision	$\Delta r_{np} = 0.22 \pm 0.04$ fm	[24]
pygmy dipole dipole polarizability	$\Delta r_{np} = 0.156 - 0.194$ fm	[15,17,25]

with quoted accuracy of ±0.024 fm

although the model dependency is still debated

and the accuracy of ±0.05 fm is taken

^{208}Pb DP $\Delta r_{np} = 0.156 - 0.021 + 0.025$ fm [17]

$\Delta r_{np} = 0.168 \pm 0.022$ fm J. Piekarewicz et al., PRC85, 041302(R) (2012)

$\Delta R_{np} = 0.165 \pm (0.009)_{expt} \pm (0.013)_{theor} \pm (0.021)_{est}$ fm X. Roca-Maza *et al.*, PRC**88**, 024316(2013)

Neutron Density (Proton Scattering)

V.E. Starodubsky et al., PRC18, 2641(1994)

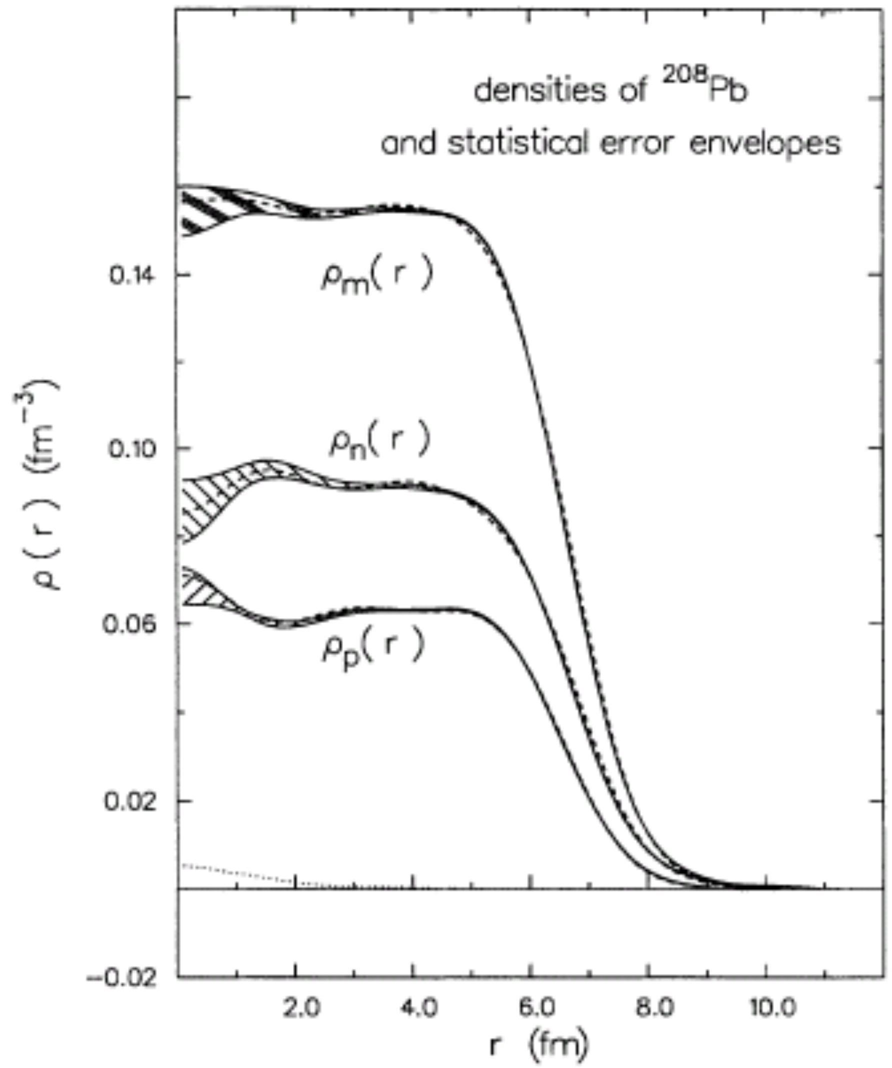

FIG. 6. Extracted neutron and matter densities for ^{208}Pb lying in the middle of the corresponding statistical error bands (the hatched areas). The HF proton, neutron, and matter densities are depicted by the dashed lines. The proton density obtained by unfolding the charge density of Ref. [43] is also shown with its statistical error envelope. The dotted line at the bottom is for the statistical error band obtained with the SOG method of Ref. [23].

R_{ch}=5.503(2), R_p=5.458, R_n=5.655(42) fm R_n-R_p=0.197(42) fm

[22] J. Zenihiro et al., PRC82, 044611 (2010)

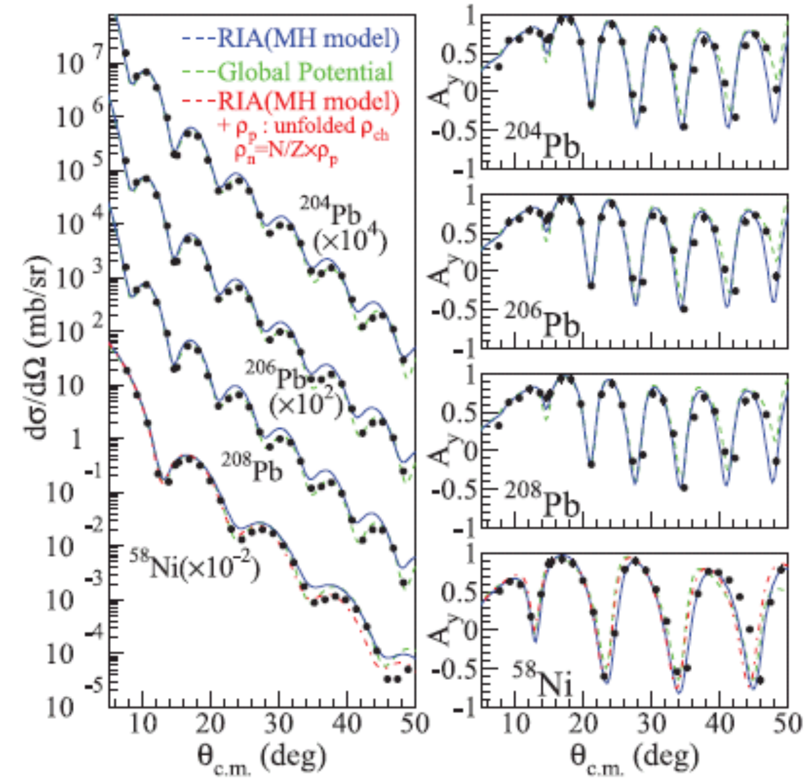

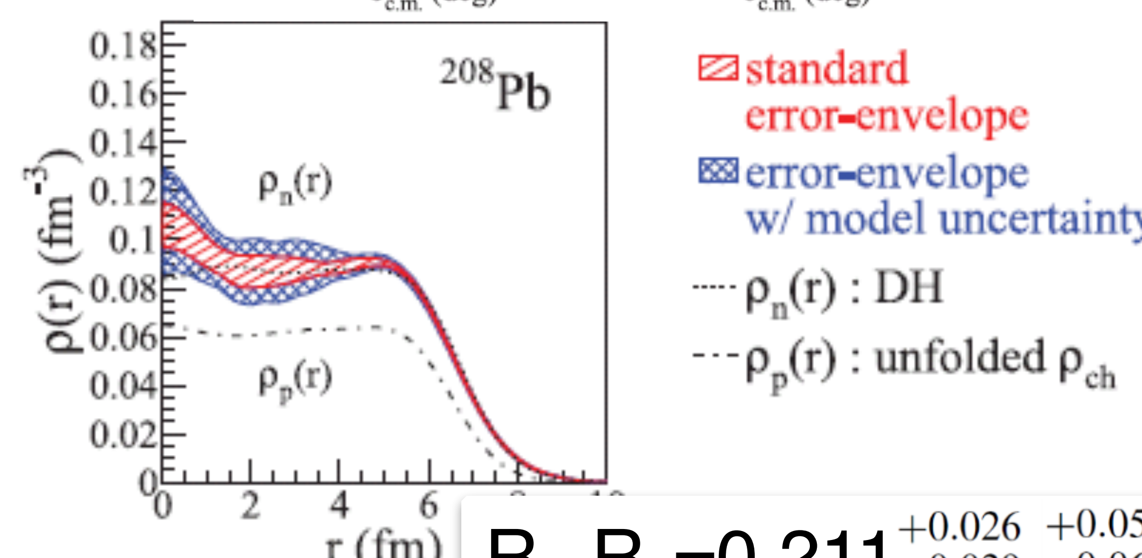

R_n-R_p=0.211$^{+0.026}_{-0.029}$ $^{+0.054}_{-0.063}$ fm

Nucleus	r_{ch}	r_p^{unfold}	r_n	δr_n^{std}	δr_n^{mdl}
^{204}Pb	5.479(2)	5.420(2)	5.598	$^{+0.029}_{-0.020}$	$^{+0.047}_{-0.059}$
^{206}Pb	5.490(2)	5.433(2)	5.613	$^{+0.026}_{-0.026}$	$^{+0.048}_{-0.064}$
^{208}Pb	5.503(2)	5.442(2)	5.653	$^{+0.026}_{-0.029}$	$^{+0.054}_{-0.063}$

Dipole Polarizability (α_D)

Dipole Polarizability is strongly correlated with R_n-R_p [17]

$$\alpha_D = \frac{\hbar c}{2\pi^2}\int \frac{\sigma_{abs}}{\omega^2}\, d\varpi = \frac{8\pi}{9}\int \frac{dB(E1)}{\omega}$$

R_n-R_p = 0.168±0.022 fm for ^{208}Pb

Determination of α_D by an Electro-Magnetic Probe

including model uncertainty.

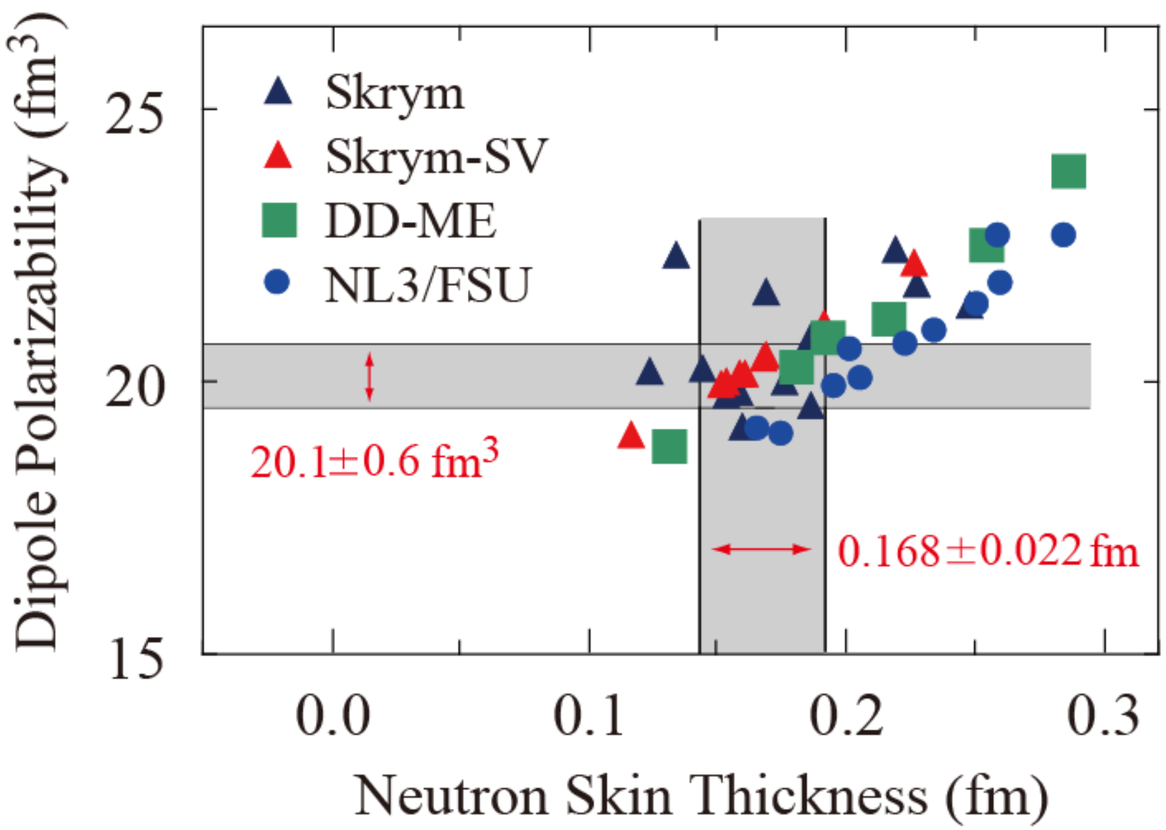

J. Piekarewicz et al., PRC85, 041302(2012)

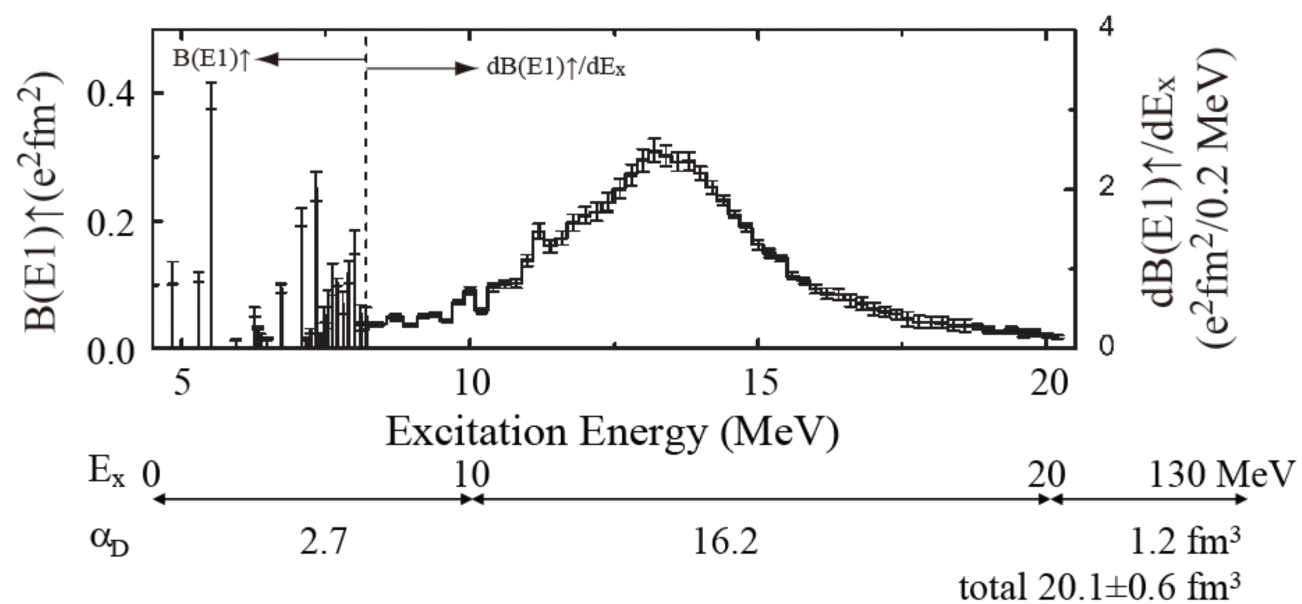

AT et al. PRL107,062502(2011) [27]

Parity Violating (PV) Cross Section Asymmetry in Electron Scattering [30]

$\sigma \approx$ 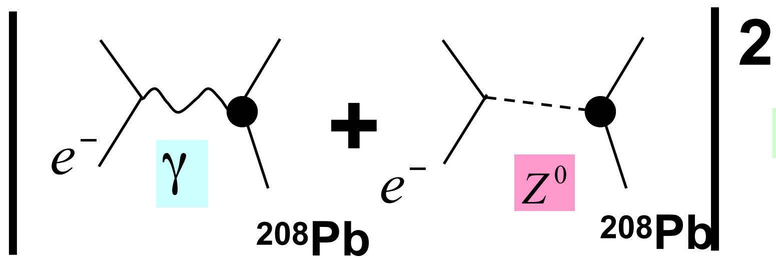

A_{PV} from interference

$$A_{\rm PV} = \frac{\sigma_R - \sigma_L}{\sigma_R + \sigma_L} \approx \frac{G_F Q^2}{4\pi\alpha\sqrt{2}} \frac{F_W(Q^2)}{F_{\rm ch}(Q^2)}, \qquad (1)$$

in PWBA

^{208}Pb

interference between EM and weak interactions

R (L): Right (Left) helicity

longitudinal polarization

G_F: Fermi coupling constant
α: fine structure constant
Q: four-momentum transfer (ω,**q**)
F_W: weak form factor
F_{ch}: charge form factor

Fourier transform of the weak charge density

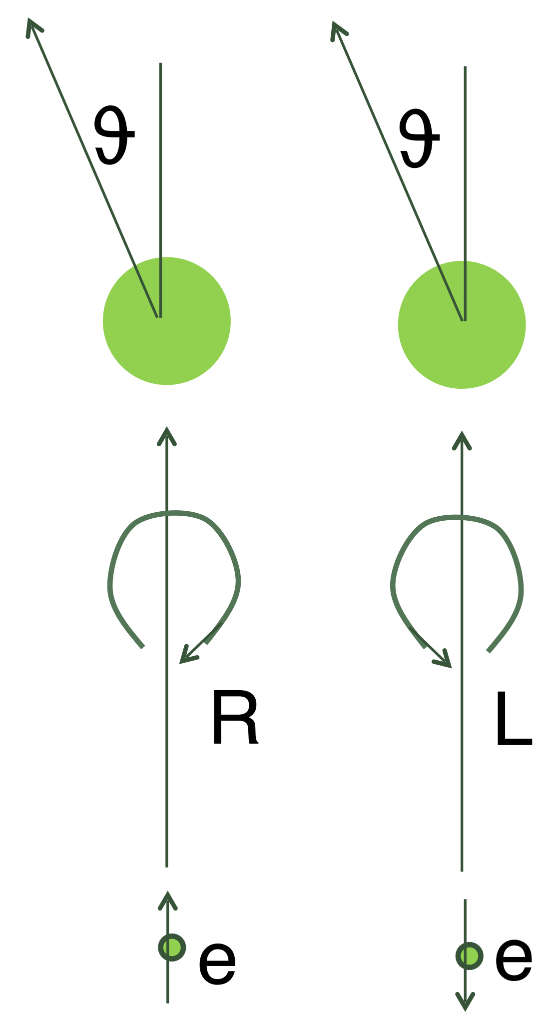

helicity

Coulomb distortion effect is included in the real analysis [9], also other effects [10].

Weak Charge

J-F. Rajotte, arxiv:1110.2218v1

TABLE I: Electroweak Couplings of u and d Quarks and Nucleons as Function of the Weak Mixing Angle θ_W in the standard model

Particles	EM Charge	Weak Charge		
u	$+\frac{2}{3}$	$1 - \frac{8}{3}\sin^2\theta_W$		
d	$-\frac{1}{3}$	$-1 + \frac{4}{3}\sin^2\theta_W$		
$p(uud)$	$+1$	$1 - 4\sin^2\theta_W$	~ 0.08	0.0721
$n(udd)$	0	-1		-0.9878

with radiative correction

ϑ_w: Weinberg Angle or Weak Mixing Angle

$\sin^2\vartheta_w$=0.23116(12) c.f. PDG 2012

$$\begin{pmatrix}\gamma \\ Z^0\end{pmatrix} = \begin{pmatrix}\cos\theta_W & \sin\theta_W \\ -\sin\theta_W & \cos\theta_W\end{pmatrix}\begin{pmatrix}B^0 \\ W^0\end{pmatrix}$$

Weak charge distribution is primarily determined by the neutron distribution

BUT weak interaction is VERY weak...

APV ~ 656 ppb = 0.000000656

Standard Model

TABLE 13.1
Weak Isospin and Hypercharge Quantum Numbers of Leptons and Quarks

Lepton	T	T^3	Q	Y
ν_e	$\frac{1}{2}$	$\frac{1}{2}$	0	-1
e_L^-	$\frac{1}{2}$	$-\frac{1}{2}$	-1	-1
e_R^-	0	0	-1	-2

Quark	T	T^3	Q	Y
u_L	$\frac{1}{2}$	$\frac{1}{2}$	$\frac{2}{3}$	$\frac{1}{3}$
d_L	$\frac{1}{2}$	$-\frac{1}{2}$	$-\frac{1}{3}$	$\frac{1}{3}$
u_R	0	0	$\frac{2}{3}$	$\frac{4}{3}$
d_R	0	0	$-\frac{1}{3}$	$-\frac{2}{3}$

$$Q = T^3 + \frac{Y}{2}$$

$$j_\mu^{em} = J_\mu^3 + \tfrac{1}{2} j_\mu^Y .$$

Backup Slides

Electro-weak Interaction

$$-i\,g(J^i)^\mu W^i_\mu - i\,\frac{g'}{2}(j^Y)^\mu B_\mu .$$

charged fields

$$W^\pm_\mu = \sqrt{\tfrac{1}{2}}\left(W^1_\mu \mp i W^2_\mu\right)$$

neutral fields (mass eigenstates)

$$A_\mu = B_\mu \cos\theta_W + W^3_\mu \sin\theta_W \qquad \text{(massless)},$$ ⟹ Electro-Magnetic Field

$$Z_\mu = -B_\mu \sin\theta_W + W^3_\mu \cos\theta_W \qquad \text{(massive)},$$

Electro-weak neutral current interaction

$$-igJ^3_\mu (W^3)^\mu - i\frac{g'}{2} j^Y_\mu B^\mu$$

$$= -i\left(g\sin\theta_W J^3_\mu + g'\cos\theta_W \frac{j^Y_\mu}{2}\right)A^\mu \quad \Longrightarrow \quad -i\,e j^{en}_\mu A^\mu$$

$$-i\left(g\cos\theta_W J^3_\mu - g'\sin\theta_W \frac{j^Y_\mu}{2}\right)Z^\mu . \quad \Longrightarrow \quad -i\frac{g}{\cos\theta_W} J^{NC}_\mu Z^\mu$$

$$g\sin\theta_W = g'\cos\theta_W = e$$

$$J^{NC}_\mu \equiv J^3_\mu - \sin^2\theta_W\, j^{em}_\mu$$

Backup Slides

Electro-magnetic interaction

$$-i\,e\,(j^{em})^{\mu}\,A_{\mu} = -i\,e\,(\bar{\psi}\gamma^{\mu}Q\psi)\,A_{\mu}$$

Vector coupling

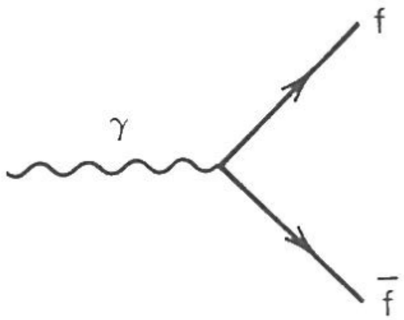

$$\boxed{-ieQ_f\gamma^{\mu}}$$

Electro-weak neutral current interaction

$$-i\frac{g}{\cos\theta_W}\left(J^3_{\mu} - \sin^2\theta_W j^{em}_{\mu}\right)Z^{\mu} =$$

$$-i\frac{g}{\cos\theta_W}\bar{\psi}_f\gamma^{\mu}\left[\underline{\tfrac{1}{2}(1-\gamma^5)}T^3 - \sin^2\theta_W Q\right]\psi_f Z_{\mu}$$

Vector coupling

V-A coupling

produces parity-violation

=L-helicity projection operator

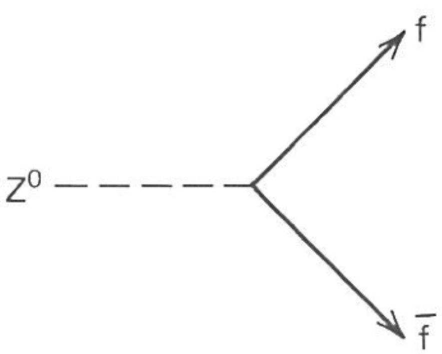

$$\boxed{-i\frac{g}{\cos\theta_W}\gamma^{\mu}\tfrac{1}{2}\left(c_V^f - c_A^f\gamma^5\right).}$$

TAI

The Z → $f\bar{f}$ Vertex Factors, (13.41), in the Standard Model (with $\sin^2\theta_W = 0.234$)

f	Q_f	c_A^f	c_V^f
$\nu_e, \nu_{\mu}, \ldots$	0	$\frac{1}{2}$	$\frac{1}{2}$
$e^-, \mu^-, \ldots$	-1	$-\frac{1}{2}$	$-\frac{1}{2} + 2\sin^2\theta_W \simeq -0.03$
u, c, ...	$\frac{2}{3}$	$\frac{1}{2}$	$\frac{1}{2} - \frac{4}{3}\sin^2\theta_W \simeq 0.19$
d, s, ...	$-\frac{1}{3}$	$-\frac{1}{2}$	$-\frac{1}{2} + \frac{2}{3}\sin^2\theta_W \simeq -0.34$

Result

$$R_n = 5.78^{+0.16}_{-0.18}$$

$$R_n - R_p = 0.33^{+0.16}_{-0.18} \text{ fm}$$

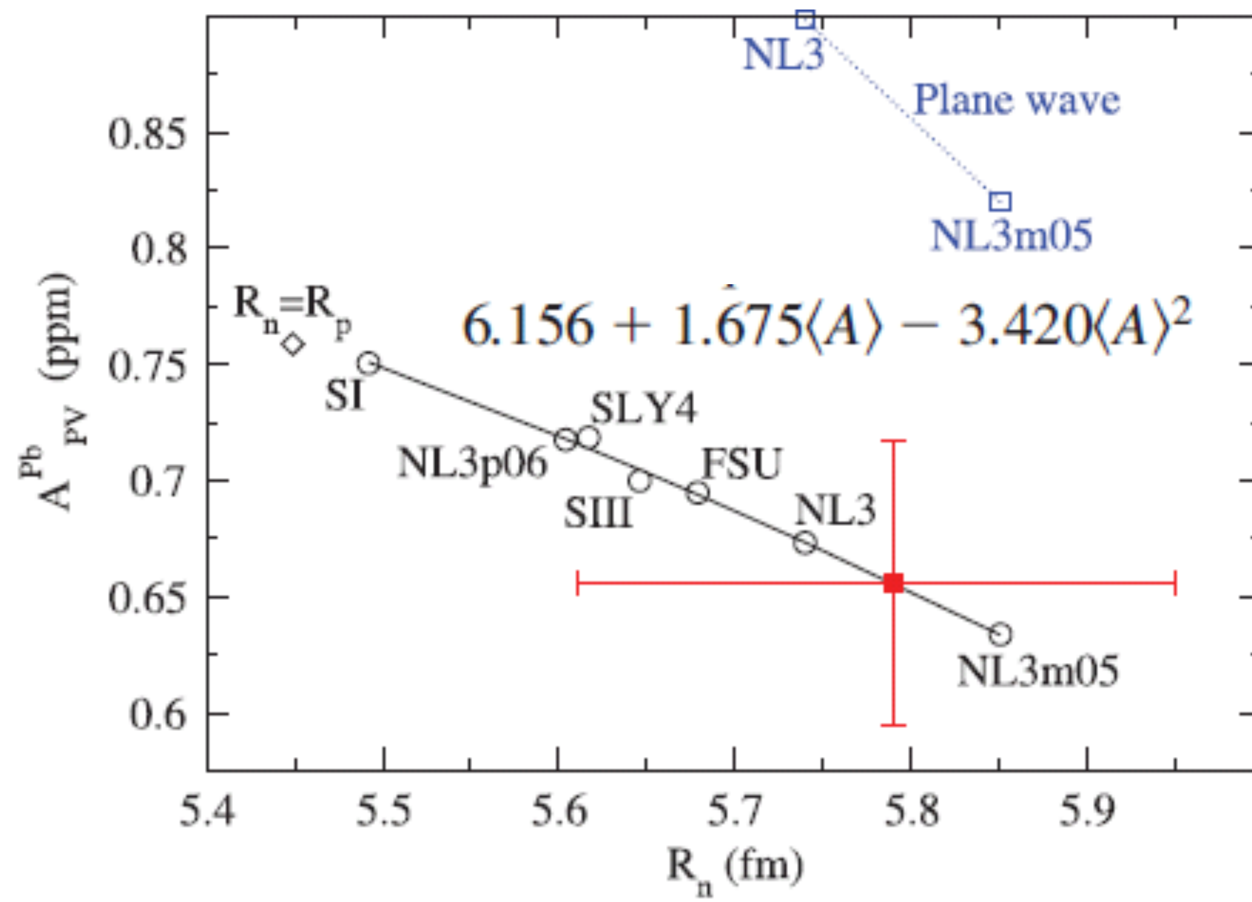

FIG. 1 (color). Result of this experiment (red square) vs neutron point radius R_n in 208Pb. Distorted-wave calculations for seven mean-field neutron densities are circles while the diamond marks the expectation for $R_n = R_p$[39]. References: NL3m05, NL3, and NL3p06 from [11], FSU from [12], SIII from [13], SLY4 from [14], SI from [15]. The blue squares show plane wave impulse approximation results.

In abstract

"provides the first electroweak observation of the neutron skin"

In summary

"A future run is planned which will reduce the quoted uncertainty by a factor of 3 [43], to discriminate between models and allow predictions relevant for the description of neutron stars and parity violation in atomic systems."

No discussion on the impact of the result?

Is this analysis really model independent?

Introductions: The case of ^{208}Pb

Experiments with electromagnetic probes [27-29]

no successful measurement on neutron density distribution

Electroweak probe: parity-violating electron scattering PREX [30]

$$\Delta r_{np} = 0.33 \pm 0.17 \text{ fm}$$

Coherent π^0 Photo-production:

- Electro-magnetic probe
- Sufficient sensitivity to the neutron skin

Coherent π^0 Photopdroduction

- Electro-magnetic probe
- Sufficient sensitivity to the neutron skin

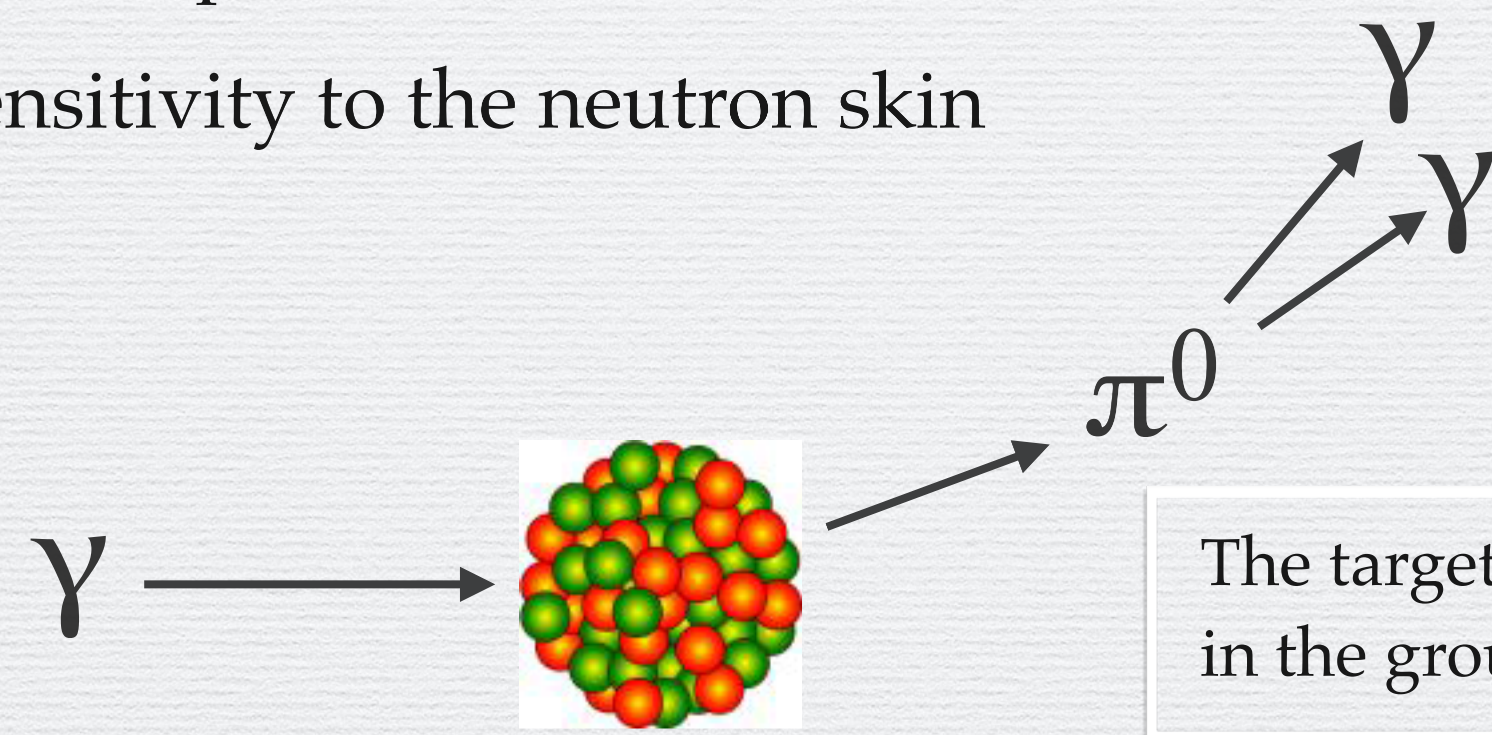

The target nucleus stays in the ground state

elementary processes

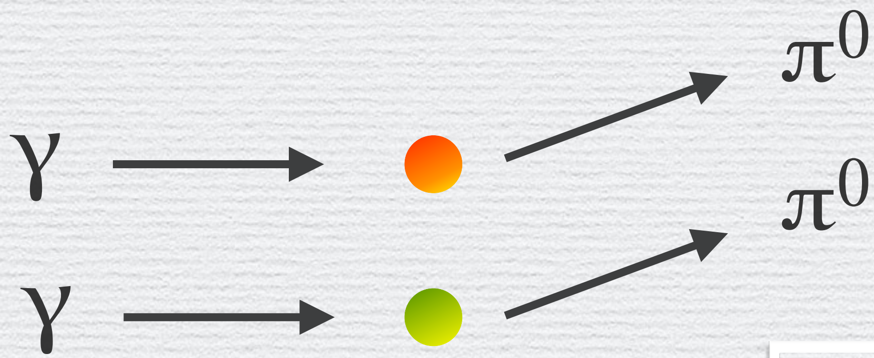

Δ excitation is the dominant process at 180-240 MeV

neutron and proton Δ excitations are expected to be identical

All the nucleons contribute coherently to the reaction amplitude

Coherent π^0 Photopdroduction

- The initial state interaction is electromagnetic and is simple
- The final state interaction between π^0 and nucleus is significant.
  $\rightarrow$ shift in the angle and modification in the flux
  $\rightarrow$ theoretical calculation
- The π0-nucleus interaction is energy dependent.
  $\rightarrow$ consistency of the density distribution at different energies
- Below 180 MeV, different photon coupling for p and n
- Above 240 MeV, the result is unreliable probably due to the rapid increase on the π0-nucleus int.

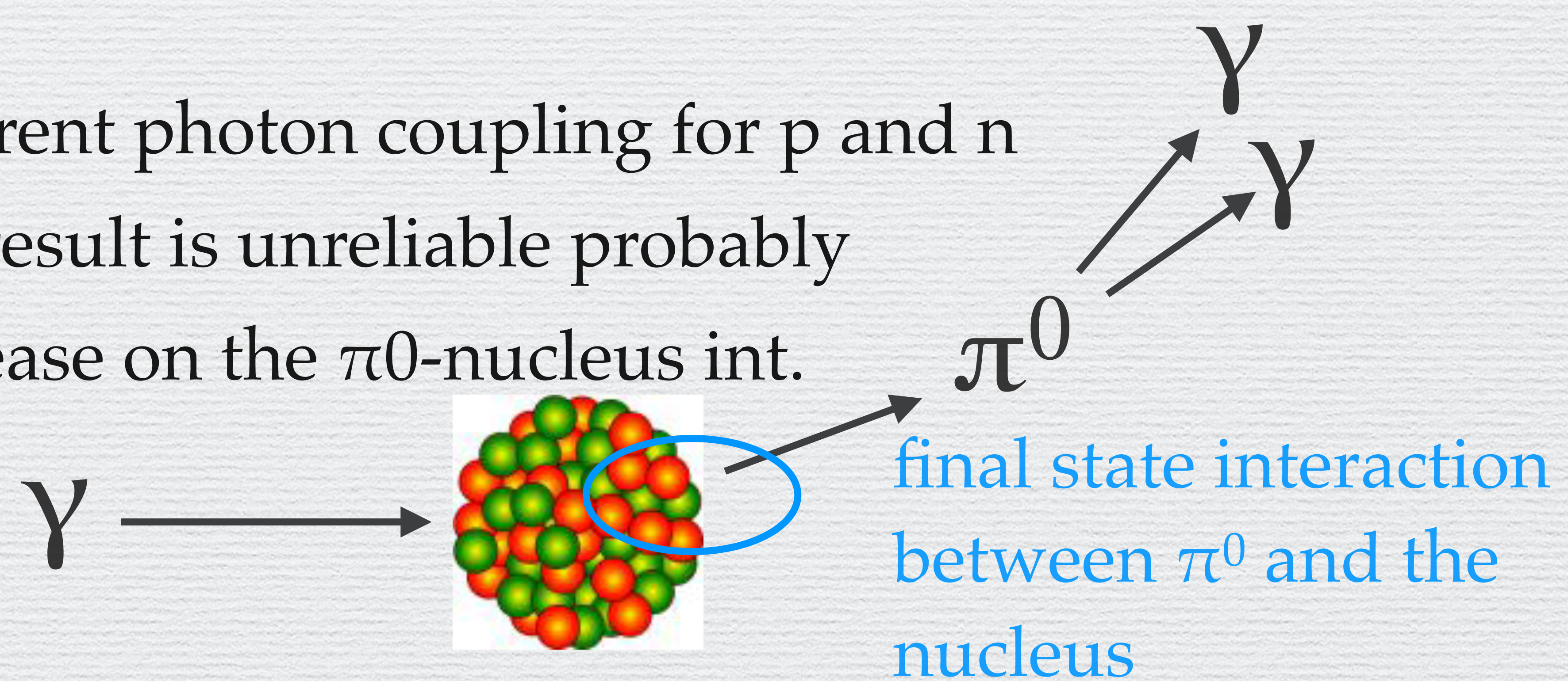

Coherent π^0 Photopdroduction

π^0 photoproduction - amplitude

- Basic production amplitude ~ equal for protons and neutrons in Δ region
- PWA (MAID,SAID) - close agreement E_γ>180 MeV for p,n cross sections
  ➔ M1 well established multipole
- Electromagnetic probe of the matter distribution!

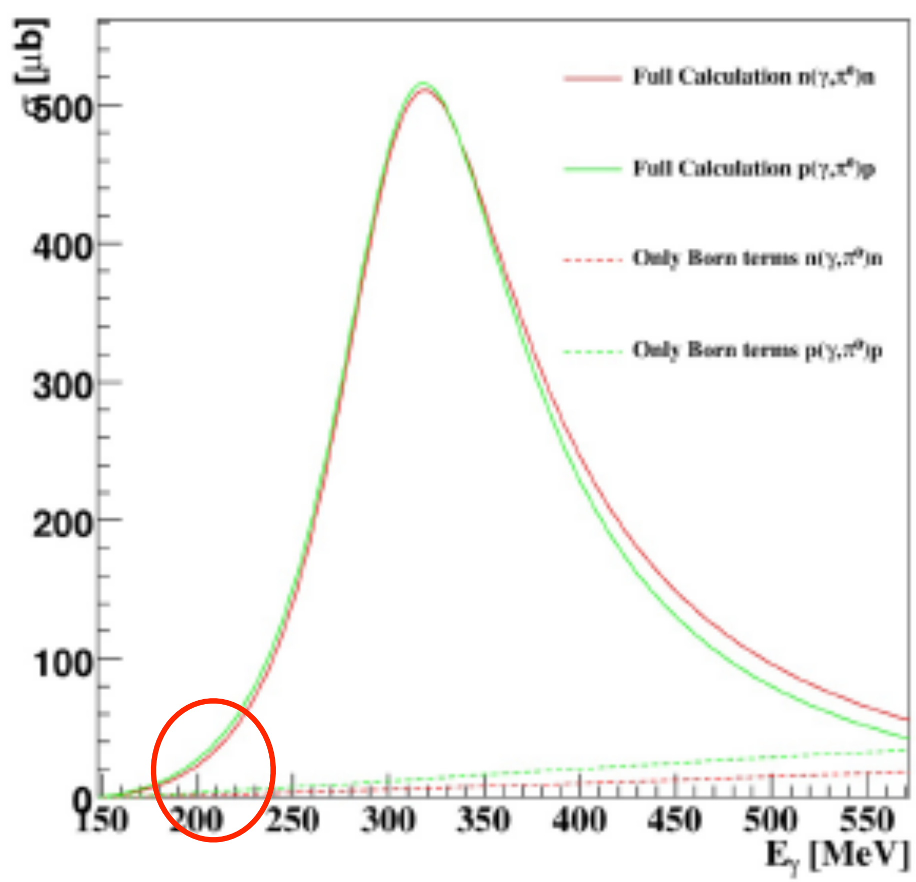

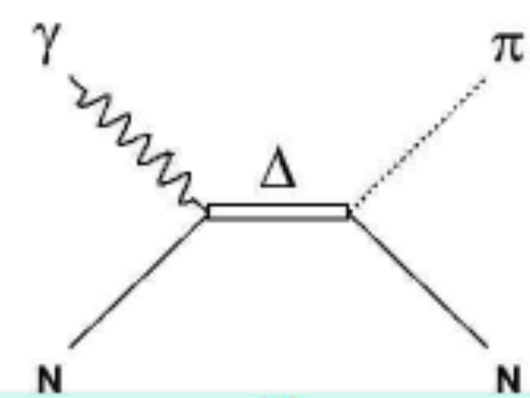

Isospin structure of amplitude

$A(\gamma p \to \pi^0 p) = \sqrt{2/3}\, A^{V3} + \sqrt{1/3}(A^{VI} - A^{IS})$
$A(\gamma n \to \pi^0 n) = \sqrt{2/3}\, A^{V3} + \sqrt{1/3}(A^{VI} + A^{IS})$

Δ has I=3/2 ➔ A^{V3} **only**
EM couplings identical for p,n

Slide by D.P. Watts

Experiment

The MAMI facility

- 100% duty factor electron microtron
- MAMI-C 1.5 GeV upgrade
  (MAMI-B 0.85 GeV)

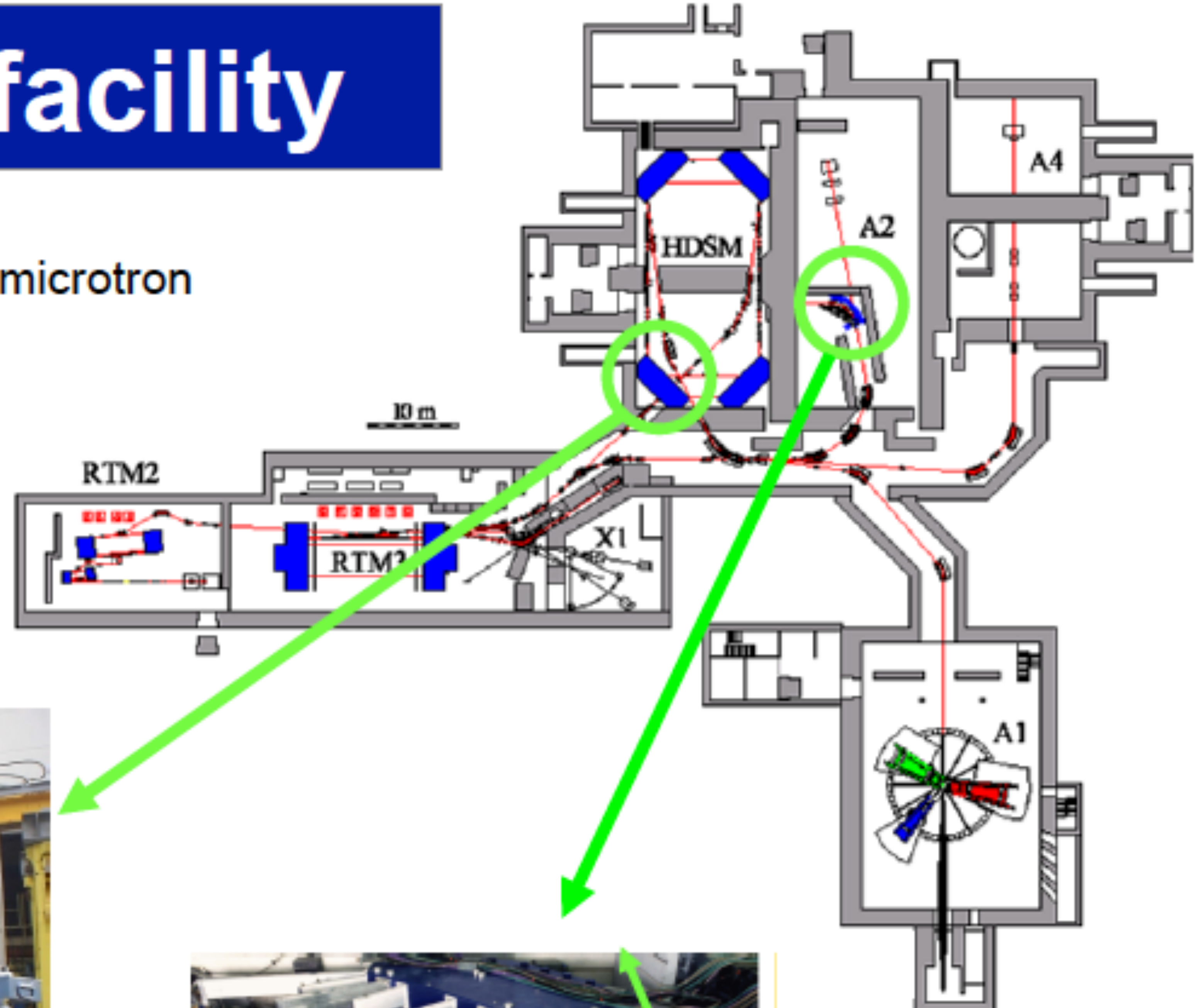

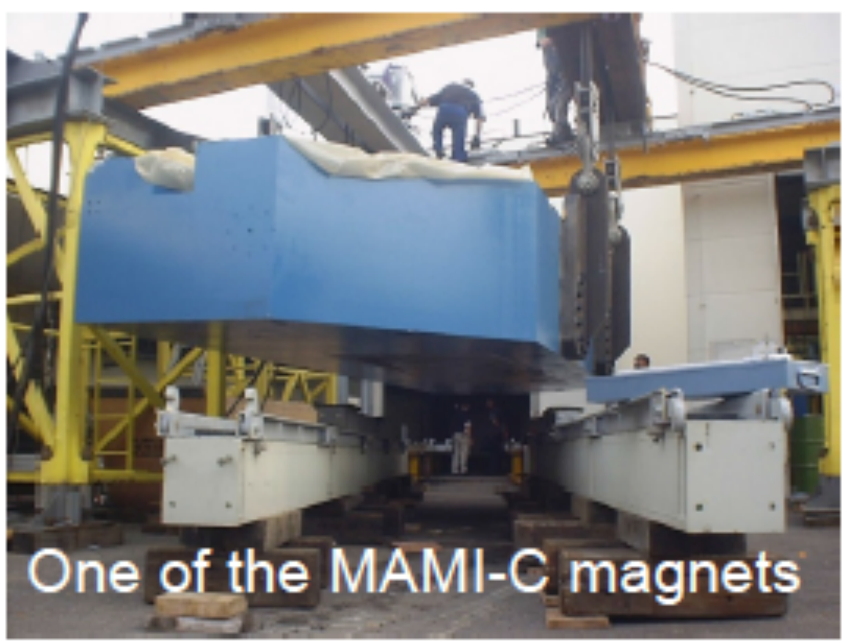
One of the MAMI-C magnets

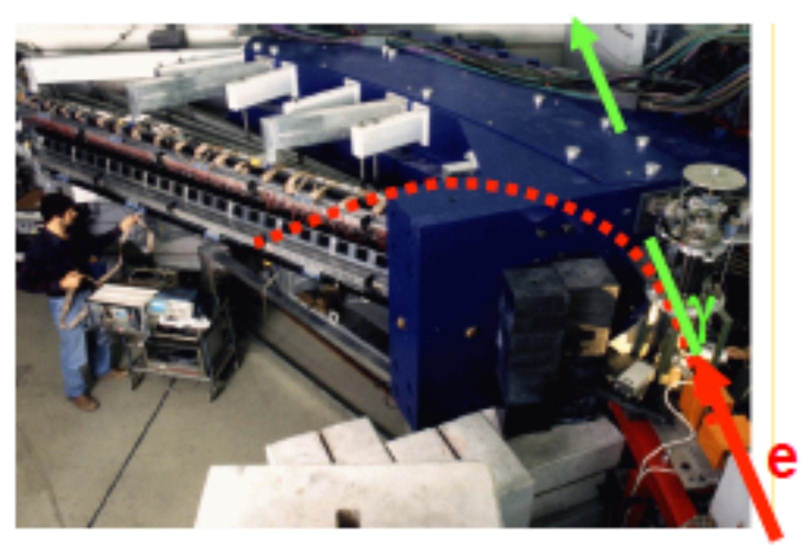

Slide by D.P. Watts

Experiment

The Mainz Microtron MAMI, scheme

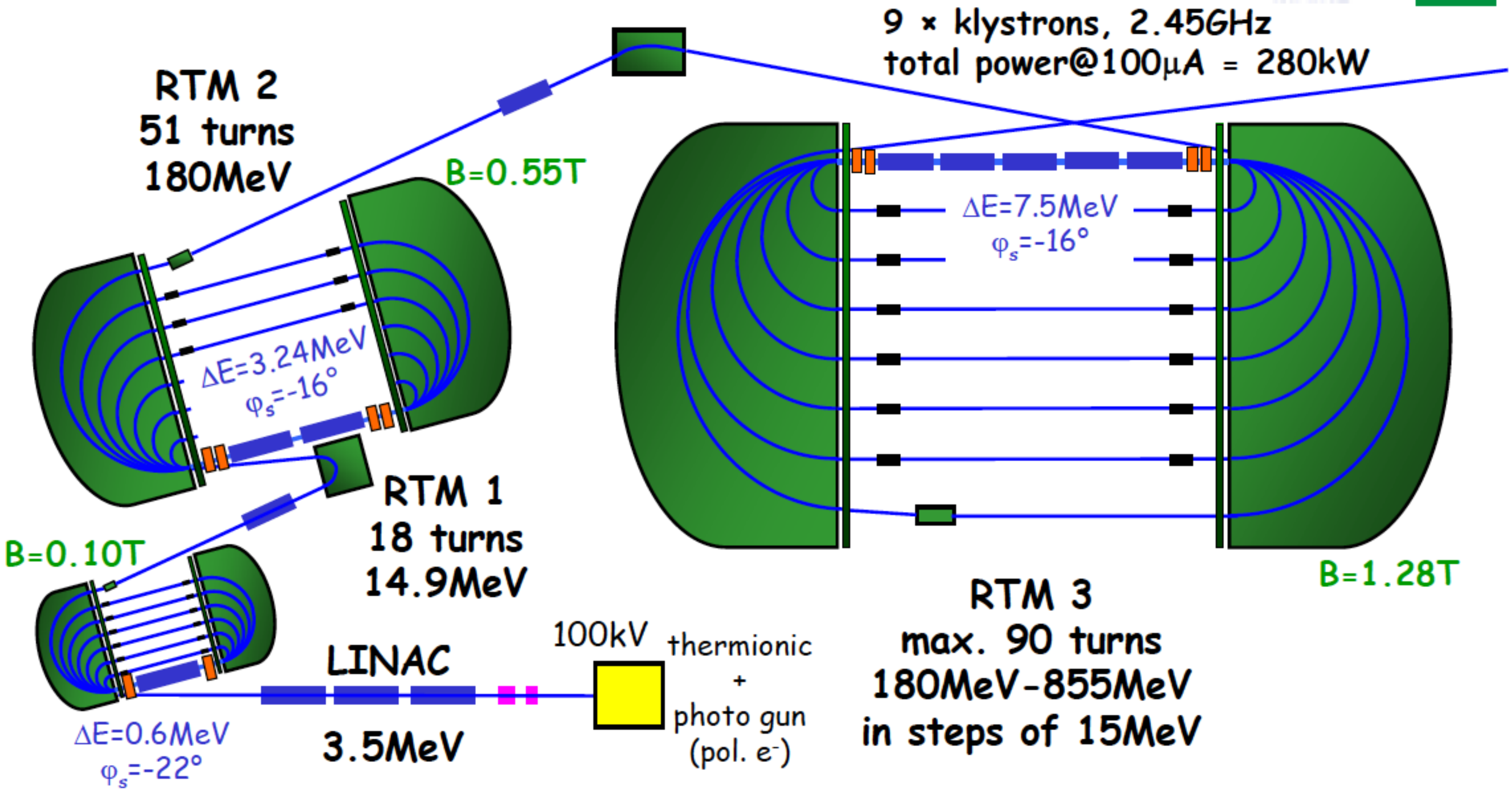

beam parameters: 100μA max cw current (86kW beam power)

injector linac:		RTM 1:		RTM 2:	*)	RTM 3:
σE=1.2keV ($3\cdot10^{-4}$)	→	σE=1.2keV ($8\cdot10^{-5}$)	→	σE=2.8keV ($1.5\cdot10^{-5}$)	→	σE=13keV ($1.5\cdot10^{-5}$)
$\varepsilon_{x,n}=0.05\cdot10^{-6}$ m rad		$\varepsilon_{x,n}=0.07\cdot10^{-6}$ m rad		$\varepsilon_{x,n}=0.25\cdot10^{-6}$ m rad		$\varepsilon_{x,n}=13\cdot10^{-6}$ m rad
						$\varepsilon_{x,abs}=8\cdot10^{-9}$ m rad

*) Increase in energy spread and emittance due to sr-effects

Experiment

RTM3

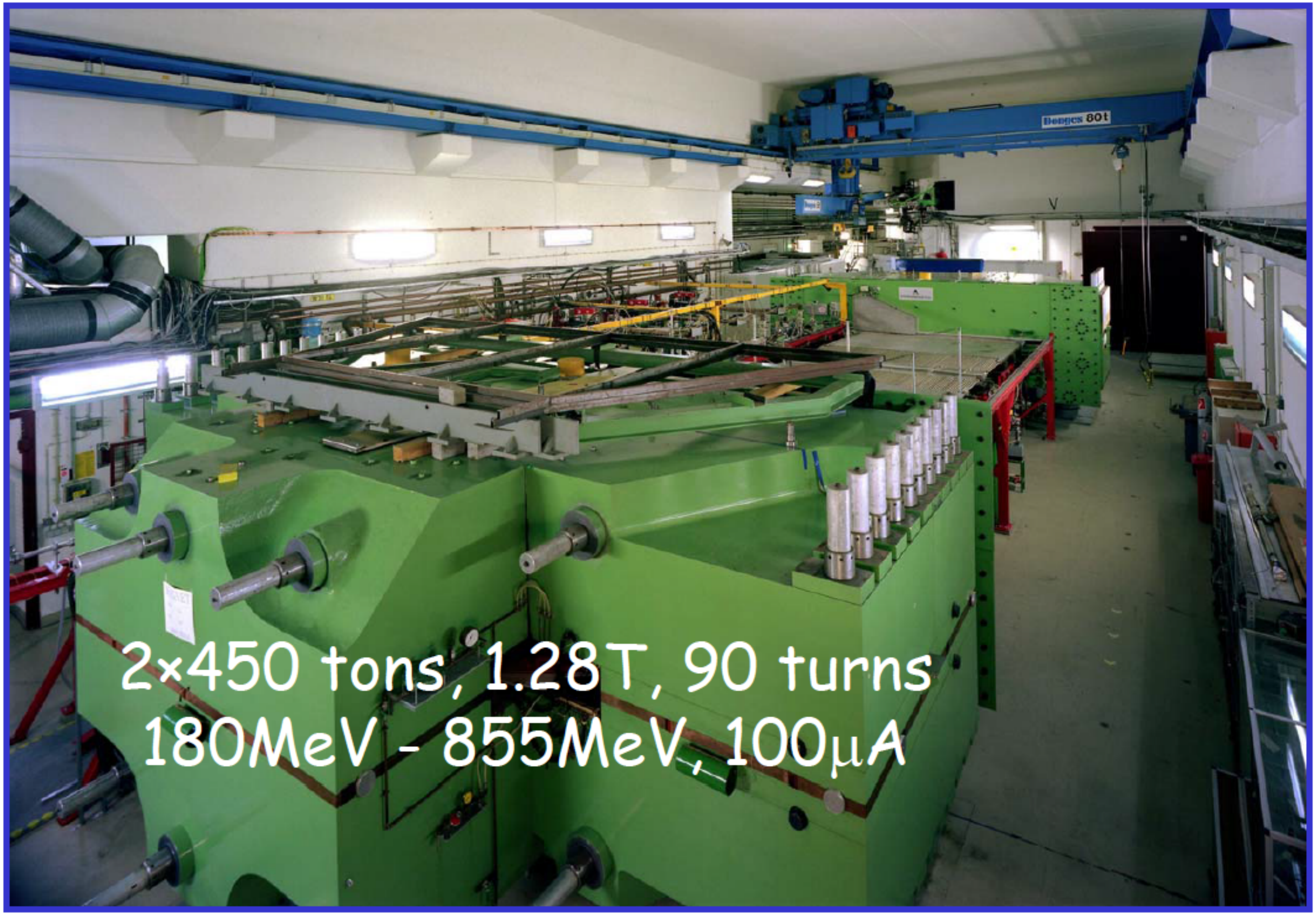

Experiment

The Harmonic Double Sided Microtron (HDSM) for MAMI C

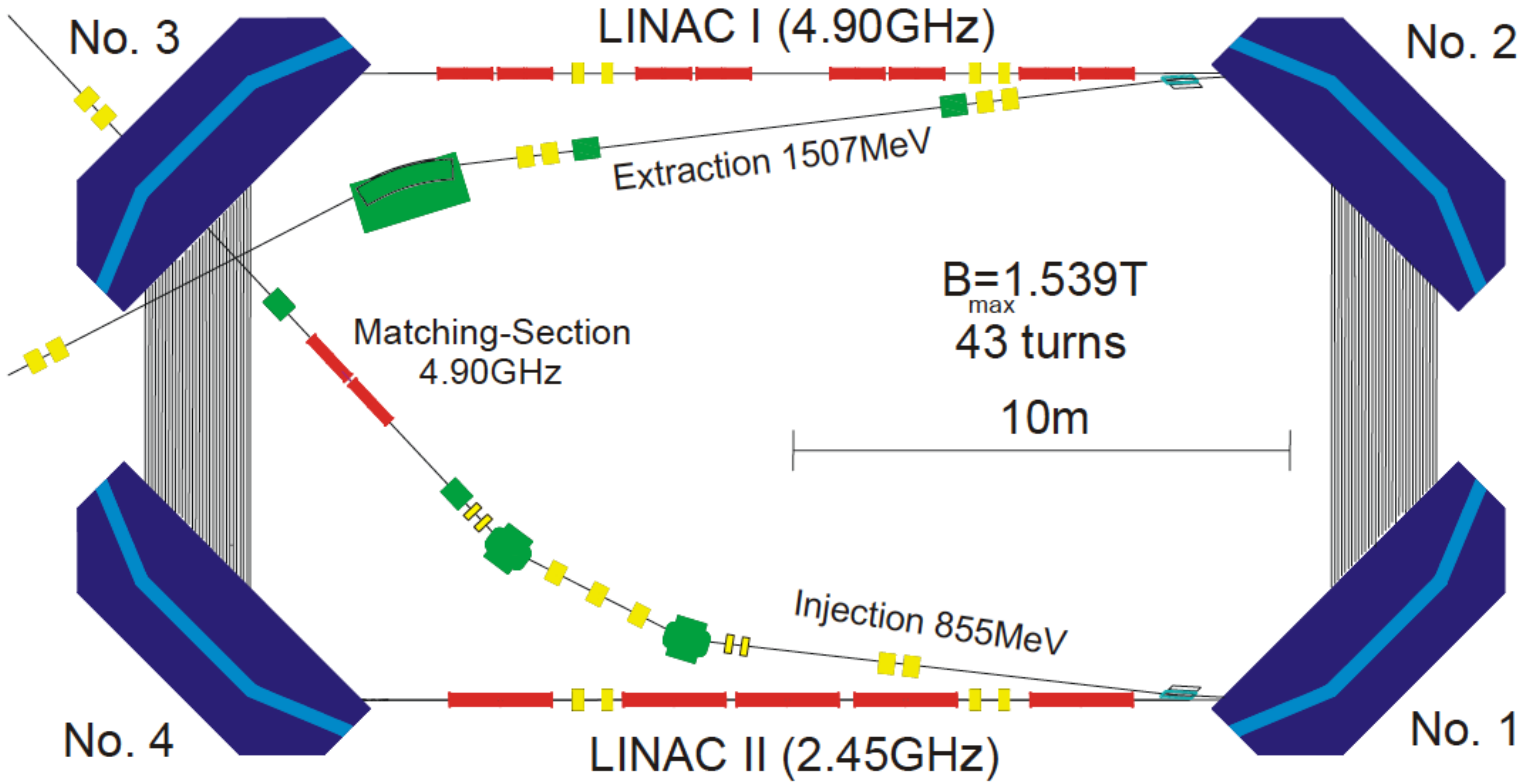

Best adaptation to the inherent stable and reliable RTM principle

Experiment

MAMI electron microtron [33]

Table 1
Main parameters of the HDSM

General			
Injection energy (MeV)	854.9		
Max. extraction energy[a]	1508.5		
Number of recirculations	43		
Length of linac straights (m)	17.359		
Distance between 1 and linac 2 (m)	12.599		
n_0 (see Eq. (9))	1057		
HF-system	Linac 1		Linac 2
Operational frequency (GHz)	4.899064		2.449532
Linac amplitude (MV)	9.05		9.30
Synchronous phase at second turn	0.6°		−35.0°
Synchronous phase at last turn	−26.8°		−50.5°
Linac length (electrical) (m)	8.567		10.097
Number of sections	8		5
Number of klystrons	4		5
Rf-power per unit length (kW/m)	14.0		11.8
Beam loading at 100 μA (kW)	37.0		28.4
Total rf-power (kW)		305.00	
Total power consumption (including matching double section) (kW)		1050	
Magnet system			
Max. magnetic flux density (T)		1.5388	
Min. magnetic flux density (T)		0.939	
Min. gap distance (mm)		85	
Max. gap distance		140	
Iron mass (ton)		1044	
Copper mass (ton)		30	
Dipole current (A)		213	
Dipole voltage (V)		320	
Number of correction dipoles		$2\times4\times43+8=352$	
Number of quadrupoles		14	
Total power consumption (kW)		310	
Beam parameters			
Energy spread (1σ) at 1.5 GeV (keV)	30 at 0.855 GeV	110[a] at 1.5 GeV	
Horizontal emittance (norm., 1σ) ($\pi\times10^{-6}$ m)	13	27[a]	
Vertical emittance (norm., 1σ) ($\pi\times10^{-6}$ m)	1.2	1.2[a]	

[a] From SYTRACE simulations.

A B S T R A C T

At the Institut für Kernphysik of Mainz University a harmonic double-sided microtron (HDSM) has been built to extend the experimental capabilities for nuclear and particle physics experiments to higher excitation energies. This novel microtron variant accelerates the 0.855 GeV continuous wave (cw) electron beam of the established three-staged race track microtron (RTM) cascade MAMI B up to 1.5 GeV. It consists of two normal conducting linear accelerators (linacs) through which the electrons are guided up to 43 times by a pair of 90°-bending magnets at each end. For beam dynamical reasons the linacs operate at the harmonic frequencies of 4.90 and 2.45 GHz. The extended facility is called MAMI C.

The relatively strong vertical defocussing due to the 45°-pole face rotations (Fig. 1) at both the entrance and exit of the segment-shaped bending magnets is compensated for all recirculations by a suitable field decay in the magnets towards higher orbits. As a consequence, the energy gain of the electrons has to decrease with increasing turn number to maintain coherent acceleration. This occurs by an appropriate phase slip of the electron bunches downwards the rf-waves during the acceleration process.

In this paper the functional principle and the beam dynamical concept of the double-sided microtron (DSM) as well as the design and development of its main components are described. Finally, the results of first beam measurements taken after starting up in December 2006 are discussed.

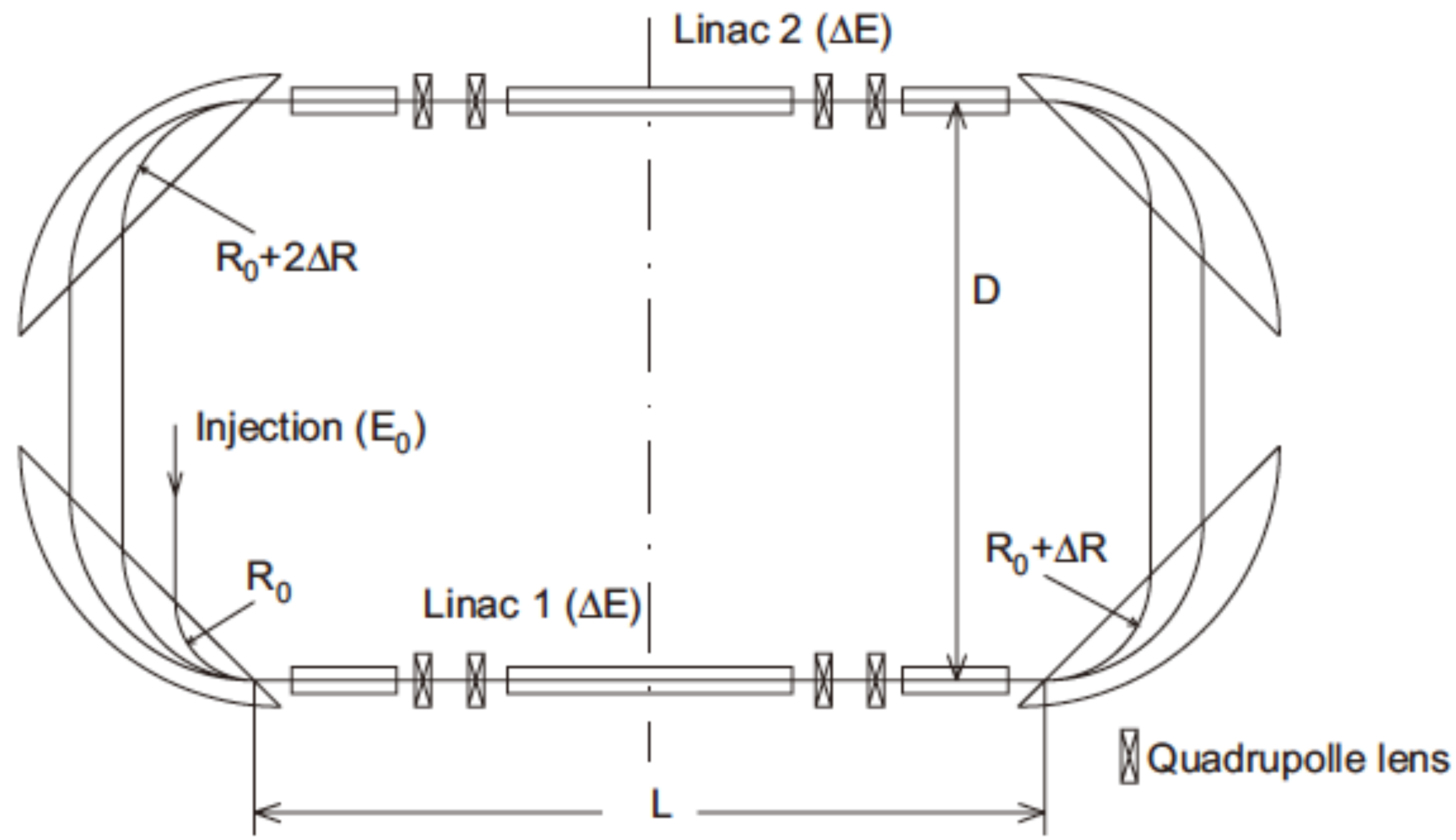

Fig. 1. Scheme of the double-sided microtron.

Experiment

Glasgow Photon Tagger [32]

2 MeV (FWHM)

$2\times10^{5}\ \gamma\ \mathrm{sec}^{-1}\ \mathrm{MeV}^{-1}$

plastic scintillators (2 mm^{t})

353 channels

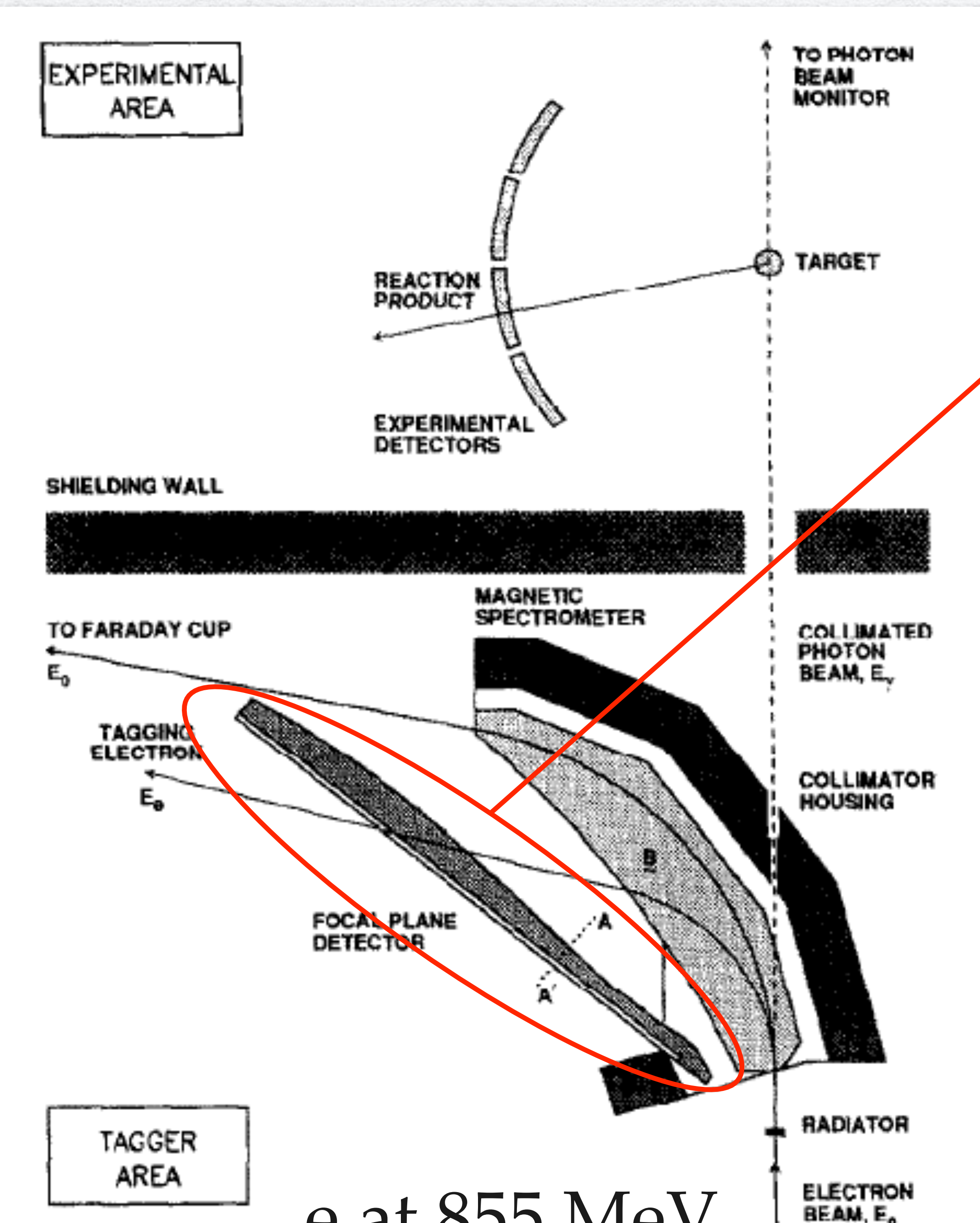

e at 855 MeV

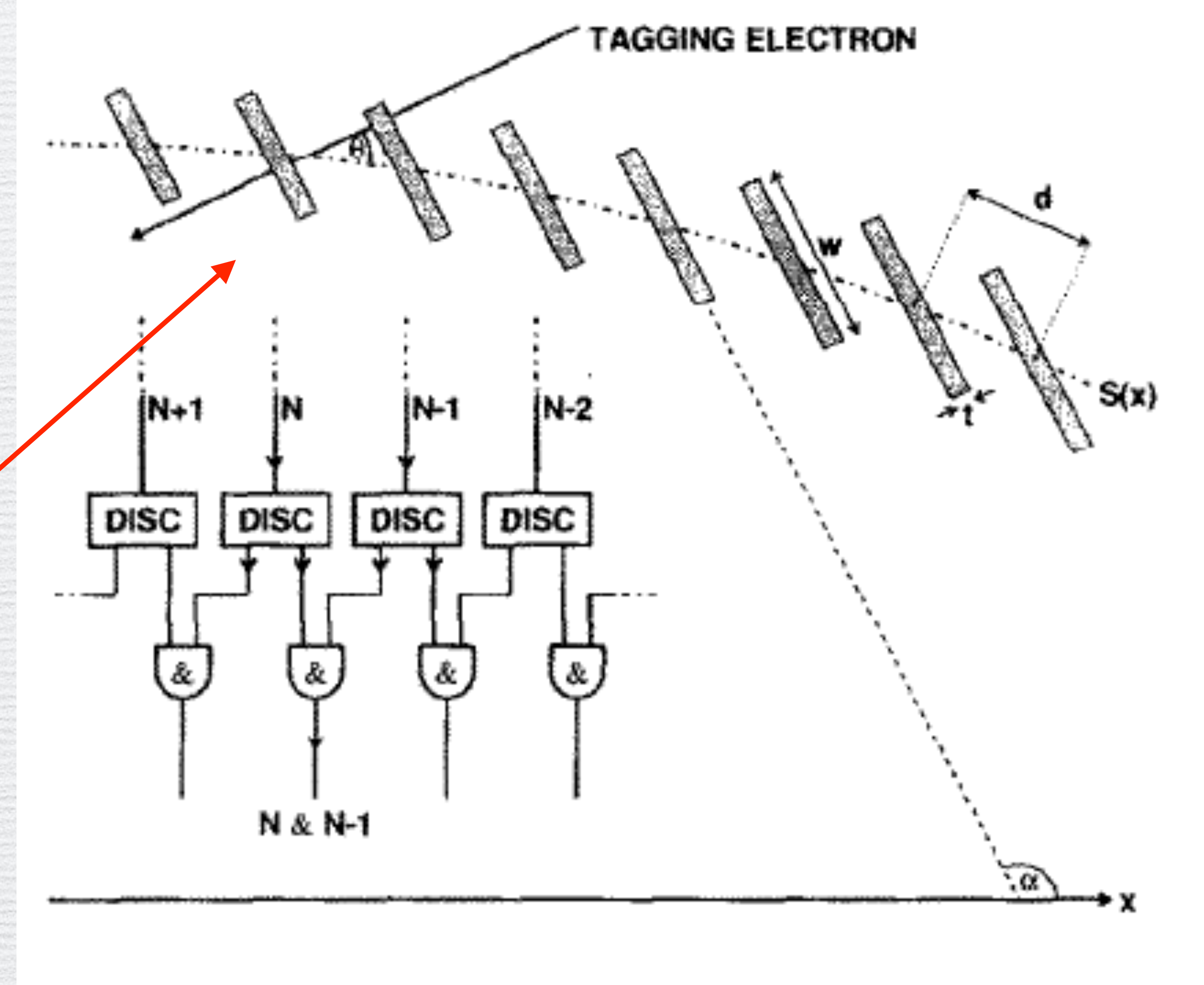

Fig. 3. Schematic view of the scintillator arrangement along the curve $S(x)$ which lies parallel to the true focal plane. The scintillators are set normal to the electron trajectories (θ) with widths (w) chosen to achieve slightly more than a half-overlap with each neighbour. The scintillator thickness (t = 2 mm) and separation (d = 13 mm) is the same for all elements. Also shown schematically is the coincidence requirement between adjacent channels.

Experiment

Glasgow Photon Tagger [32]

2 MeV (FWHM)

$2 \times 10^5\ \gamma\ \mathrm{sec}^{-1}\ \mathrm{MeV}^{-1}$

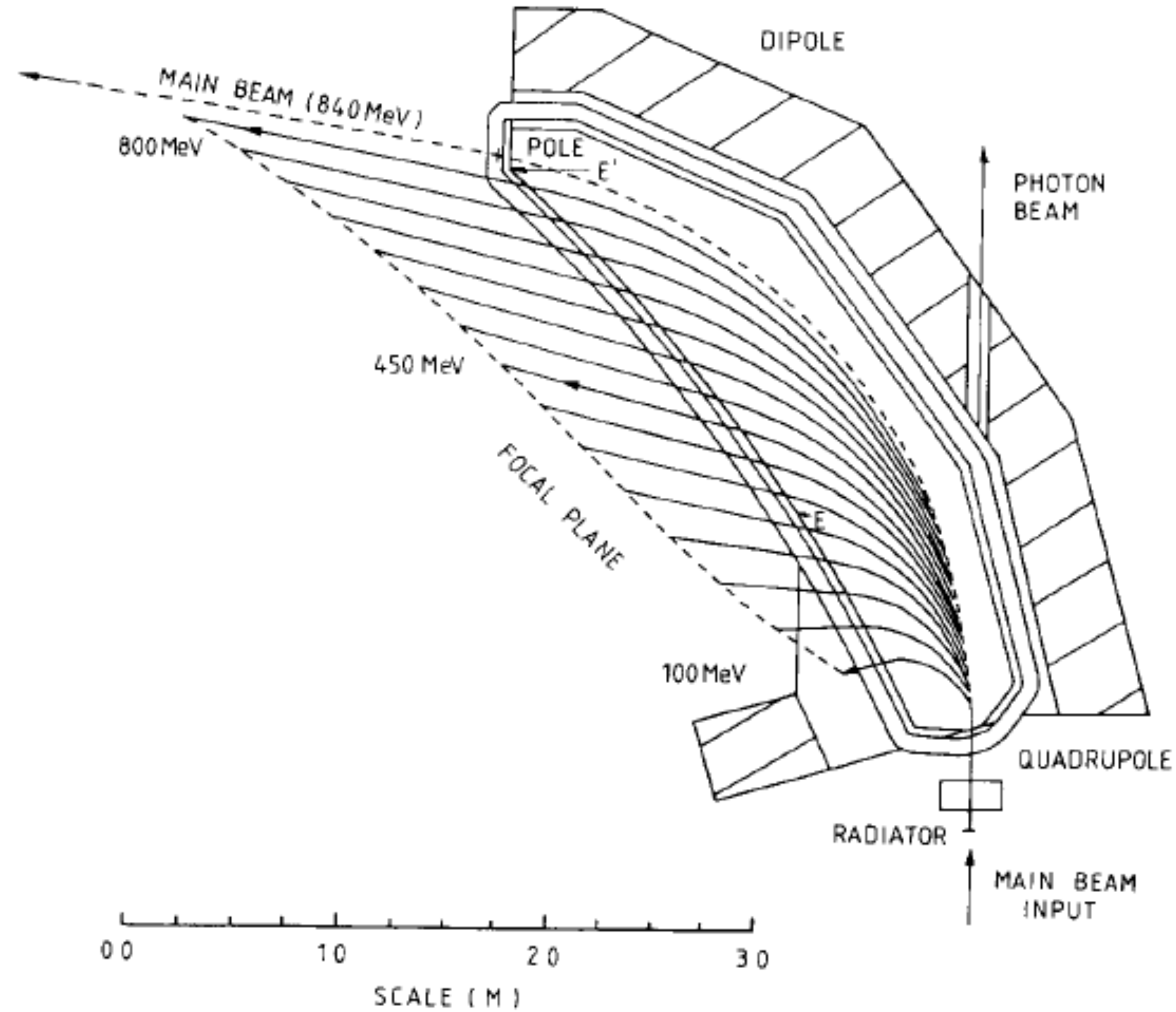

Fig. 1. Plan of the Mainz 840 MeV tagged photon spectrometer.

Experiment

Target:

^{208}Pb 99.5%, 0.52±0.01 mm thick (~590 mg/cm2)

η

Experiment

Crystal Ball (CB) [31]

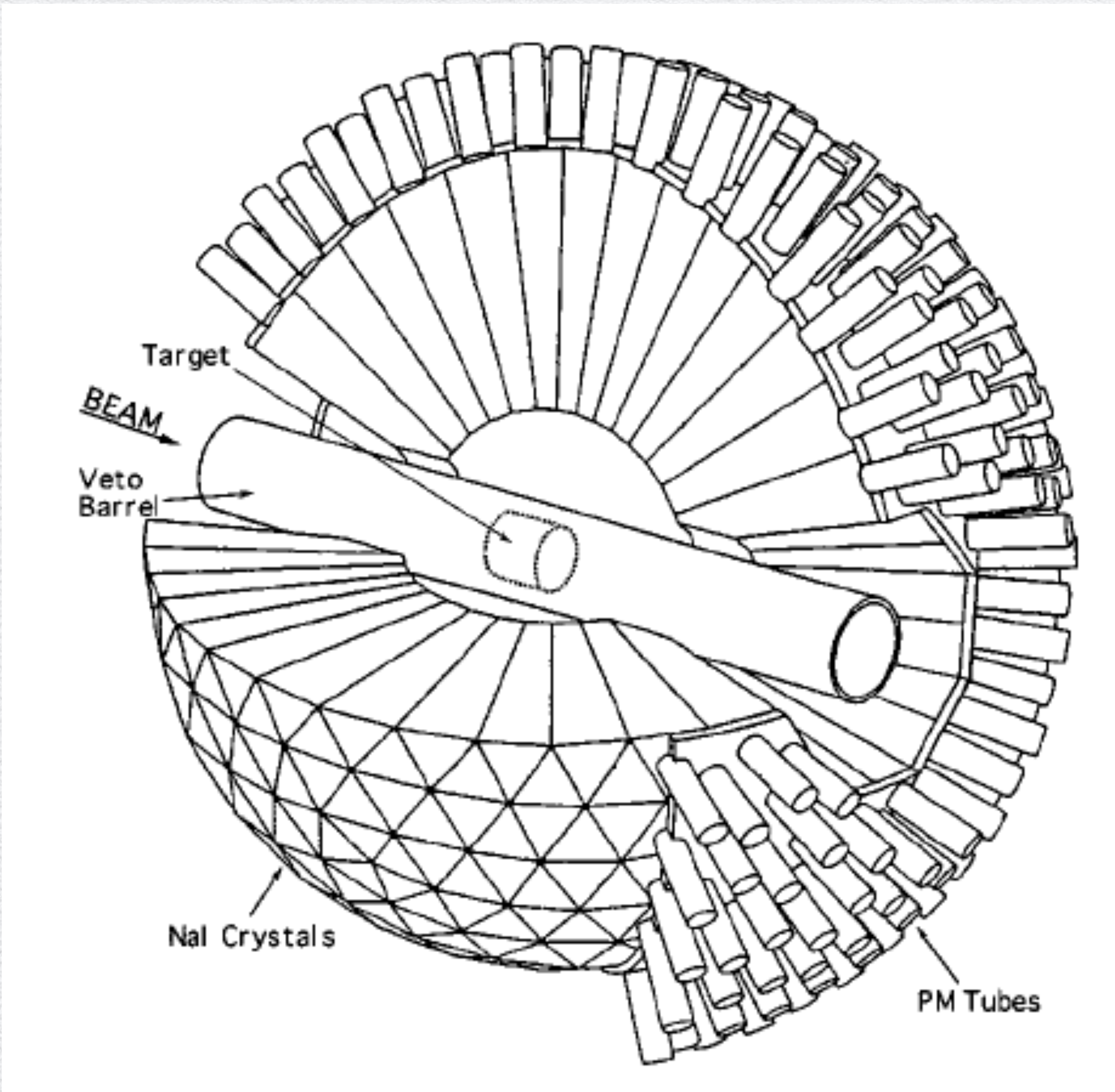

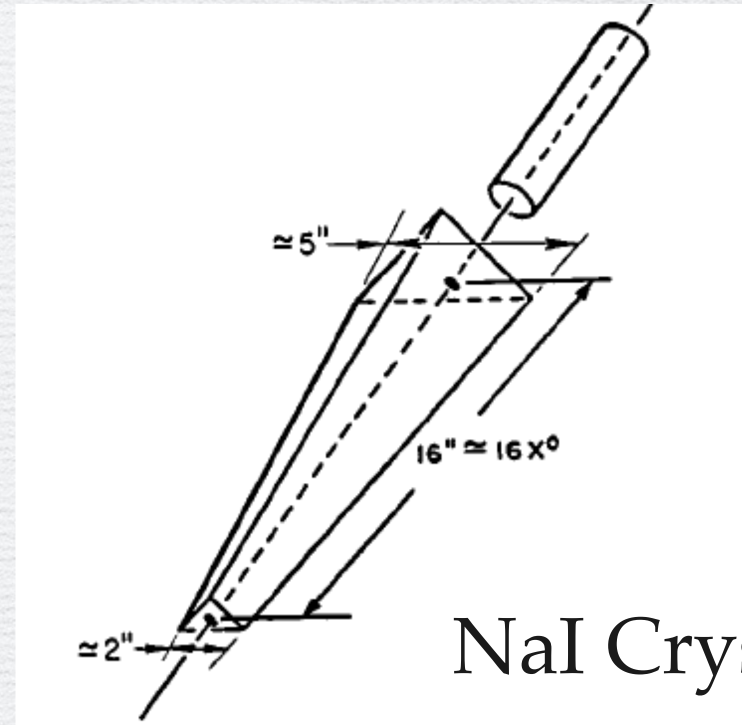

NaI Crystal

- inner radius = 25.3 cm
- outer radius = 66.0 cm
- icosahedron:
  20 triangles → 4 triangles → 9 triangles:
  692 out of 720
- wrapped with reflective paper and aluminized mylar

Experiment

Crystal Ball (CB) [31]

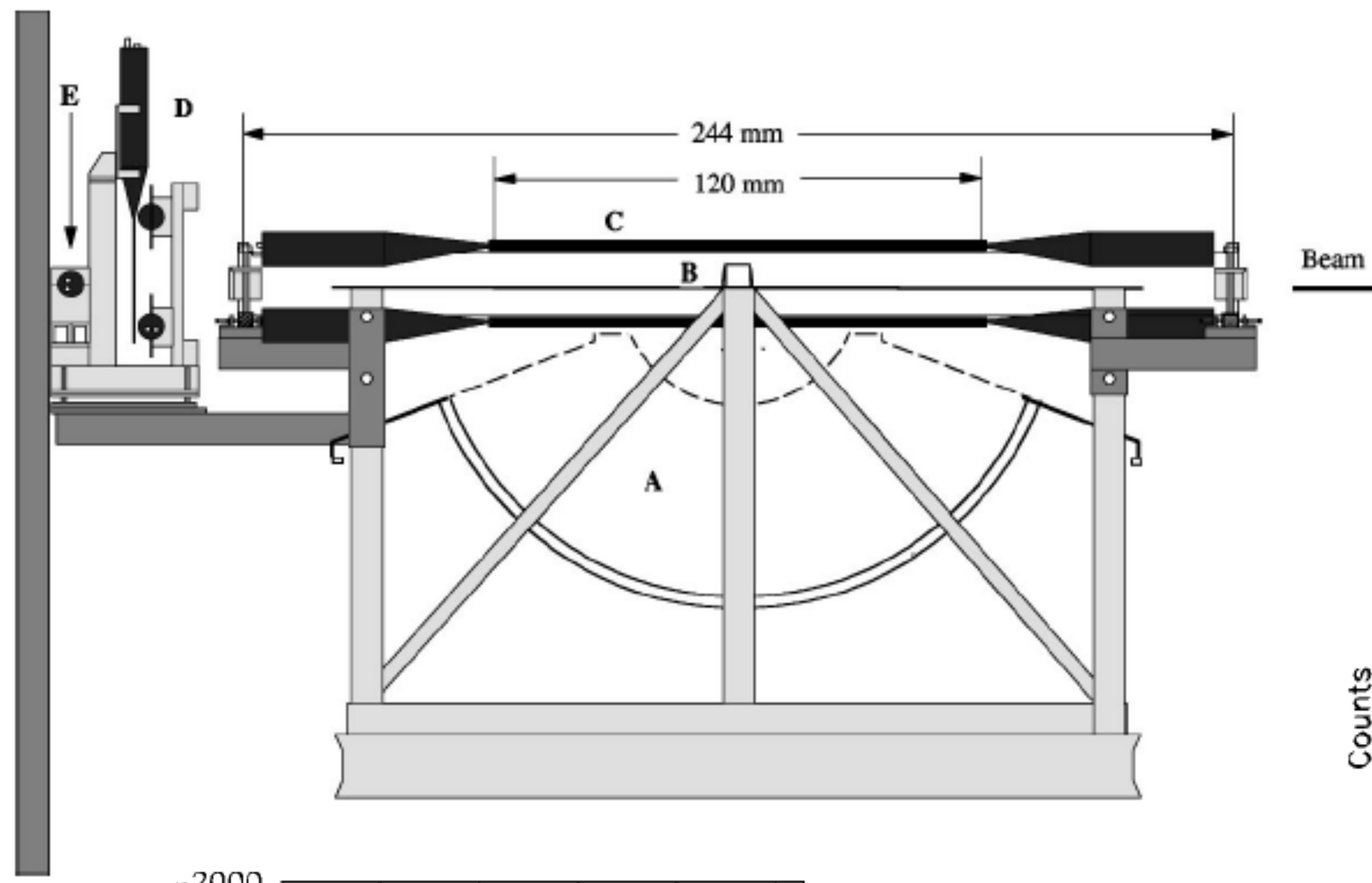

- four veto scintillators
  5mm thick and 120cm long
- 0.76 mm stainless steel
- maintained at temperature 20±1°C

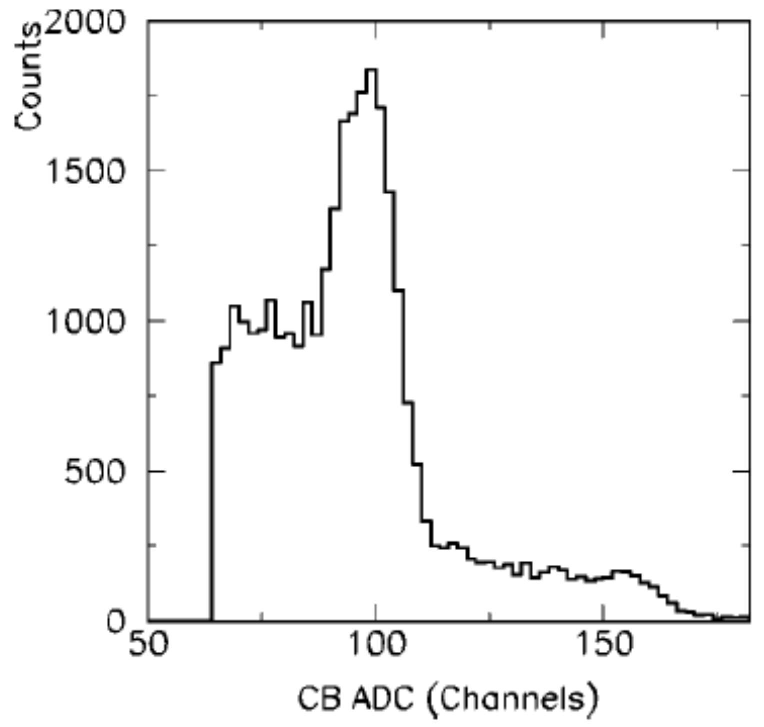

FIG. 7. Typical ^{60}Co spectrum of a CB crystal.

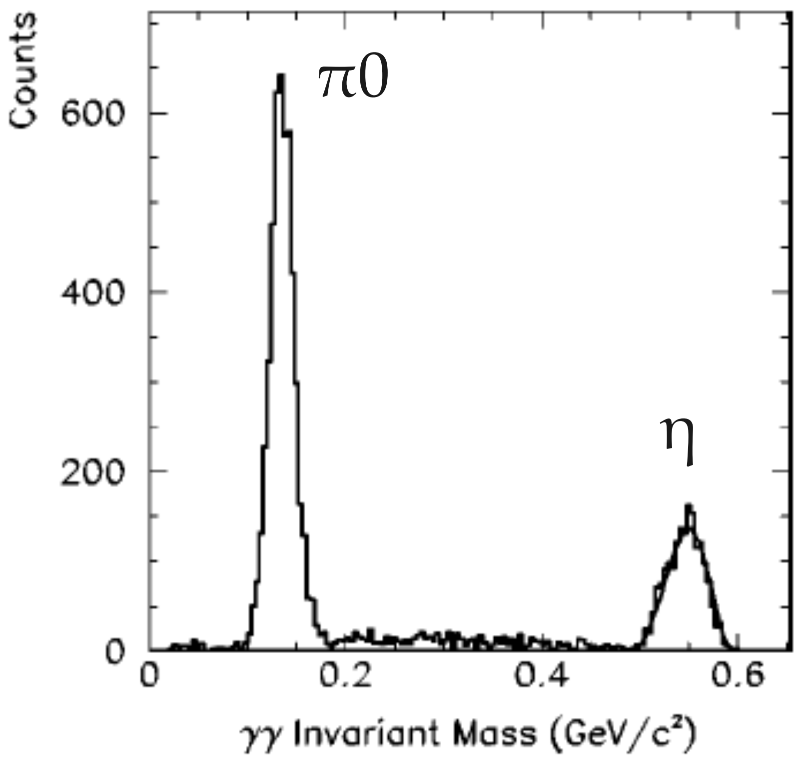

FIG. 11. The invariant mass of two photons in $K^- p \to \gamma\gamma\Lambda$ obtained with the high-momentum beam. The normalized empty target spectrum has been subtracted. The results of the Monte Carlo simulation are shown by the smooth solid line. The first peak is due to $K^- p \to \pi^0 \Lambda$ and the second one to $K^- p \to \eta\Lambda$.

Crystal Ball (CB) [31]

Experiment

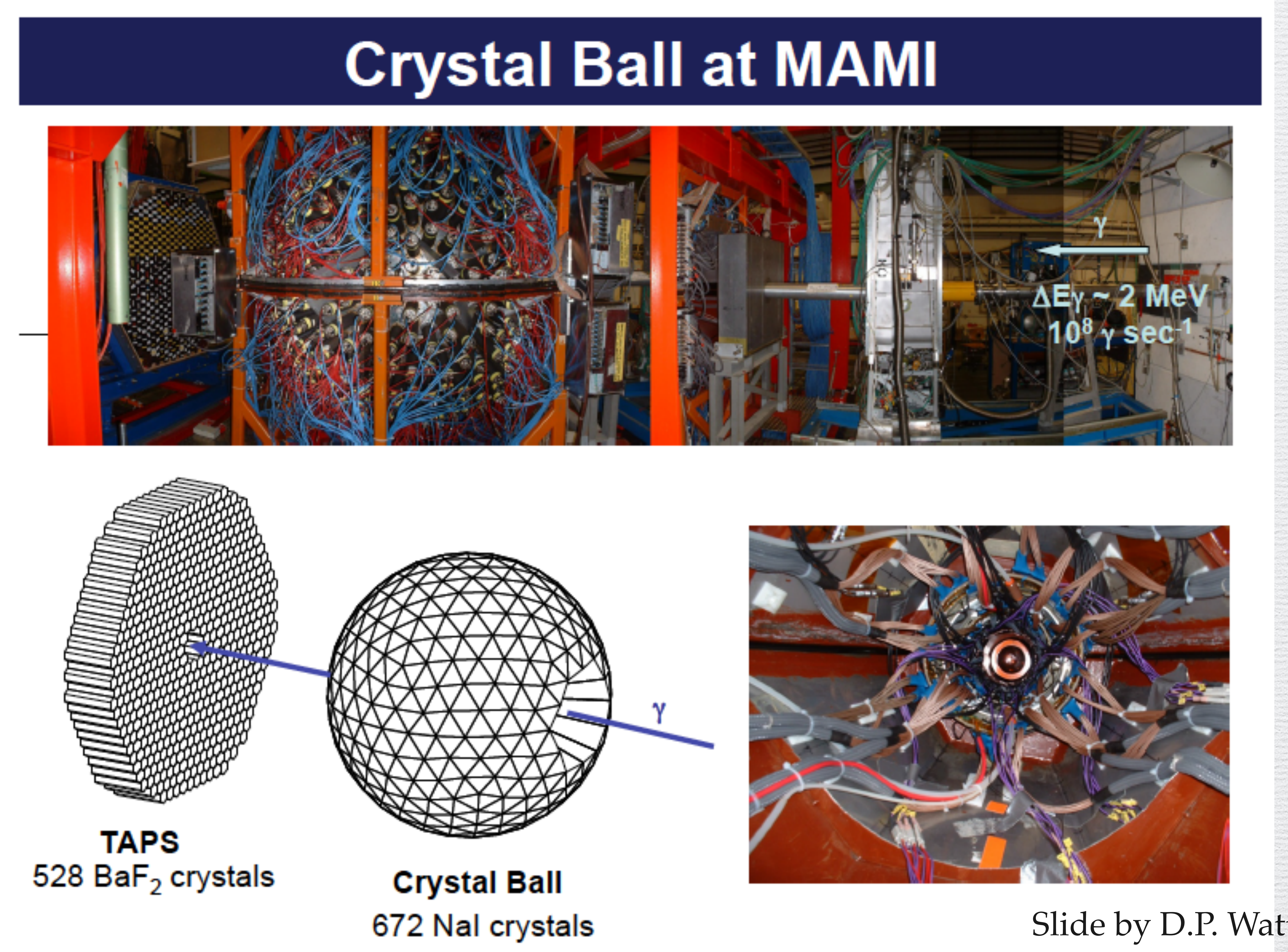

Slide by D.P. Watts

Analysis

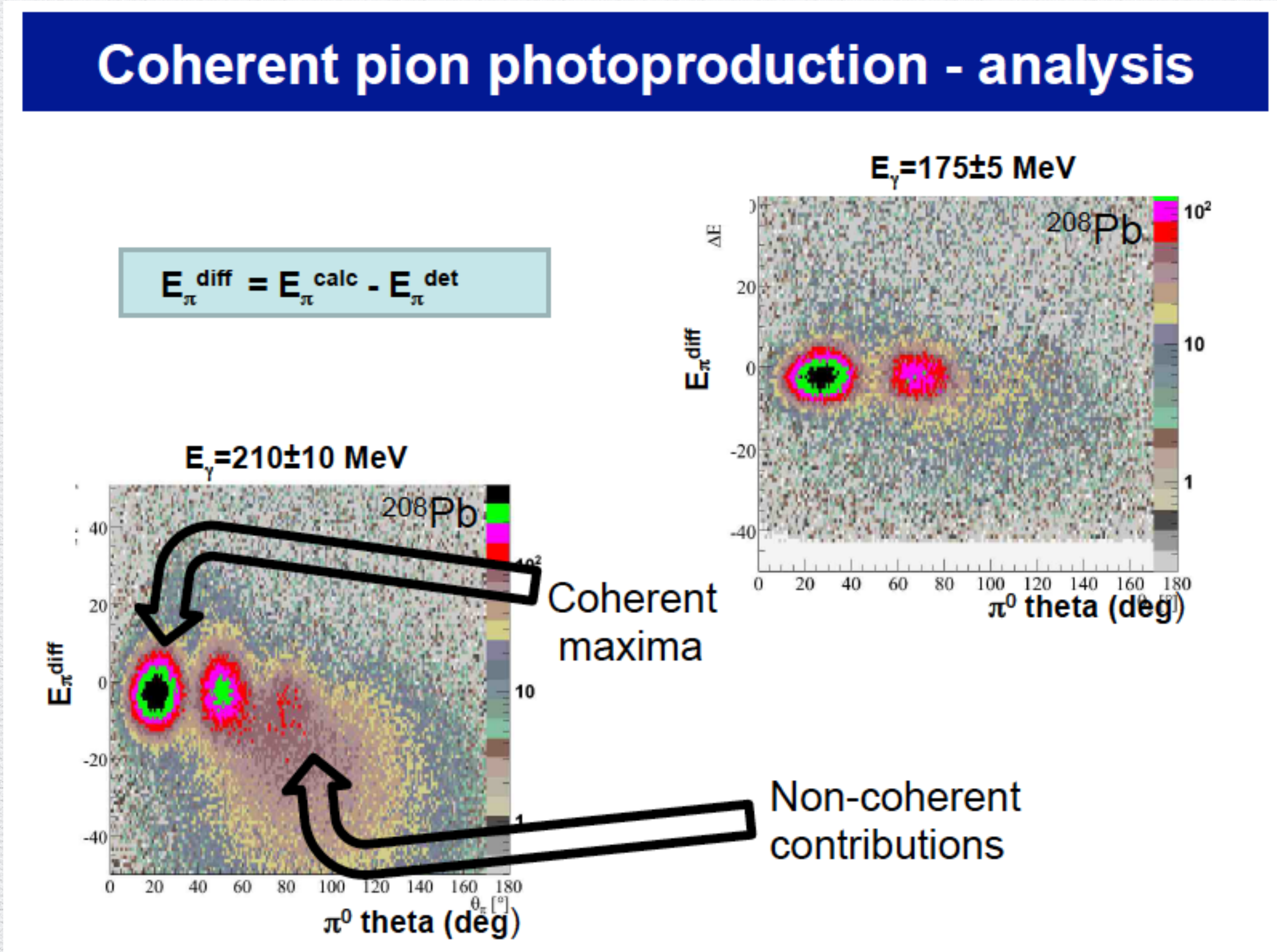

Slide by D.P. Watts

Analysis

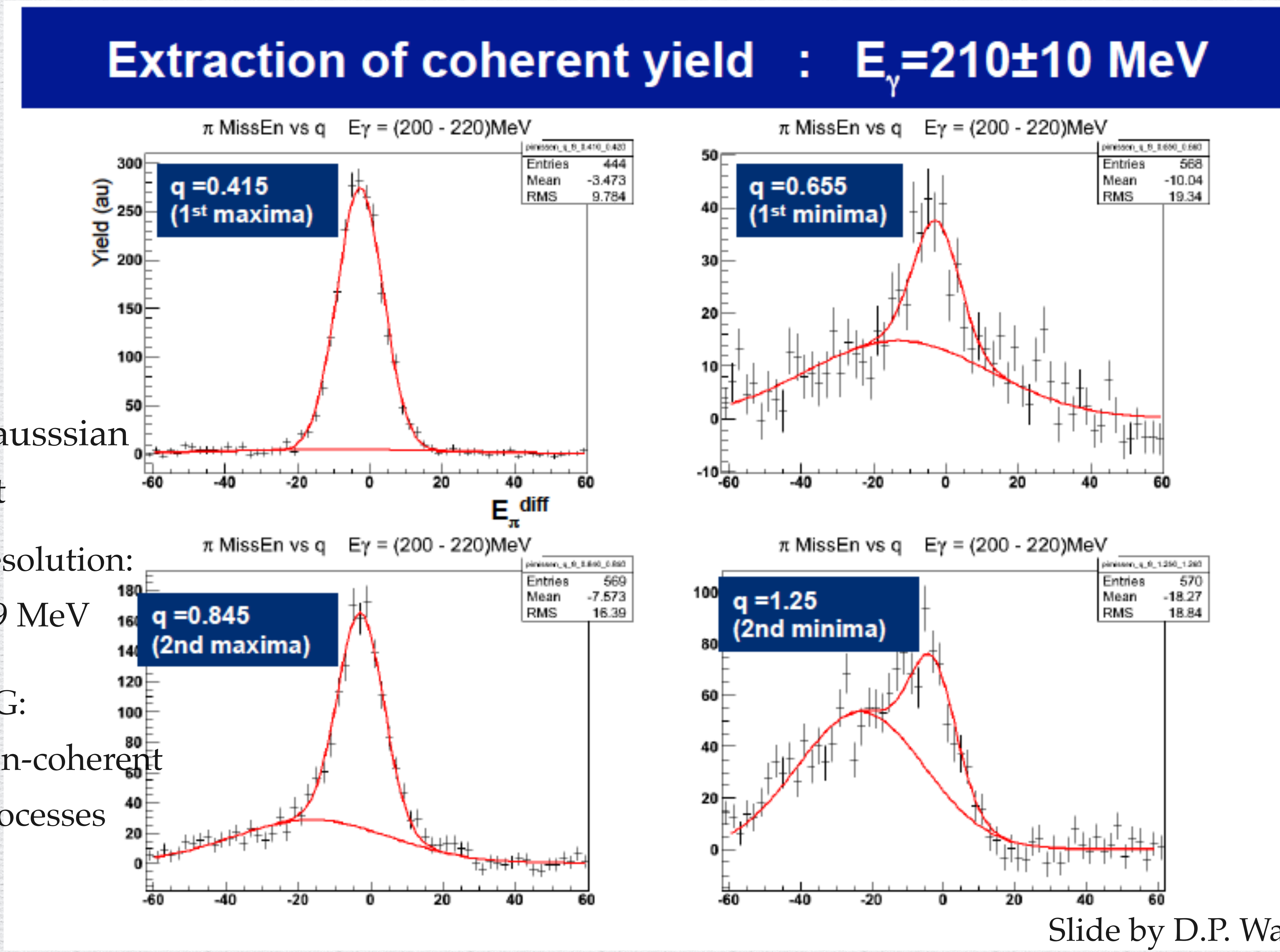

Gausssian Fit

Resolution: 2-9 MeV

B.G: non-coherent processes

Slide by D.P. Watts

Analysis

Momentum transfer distributions

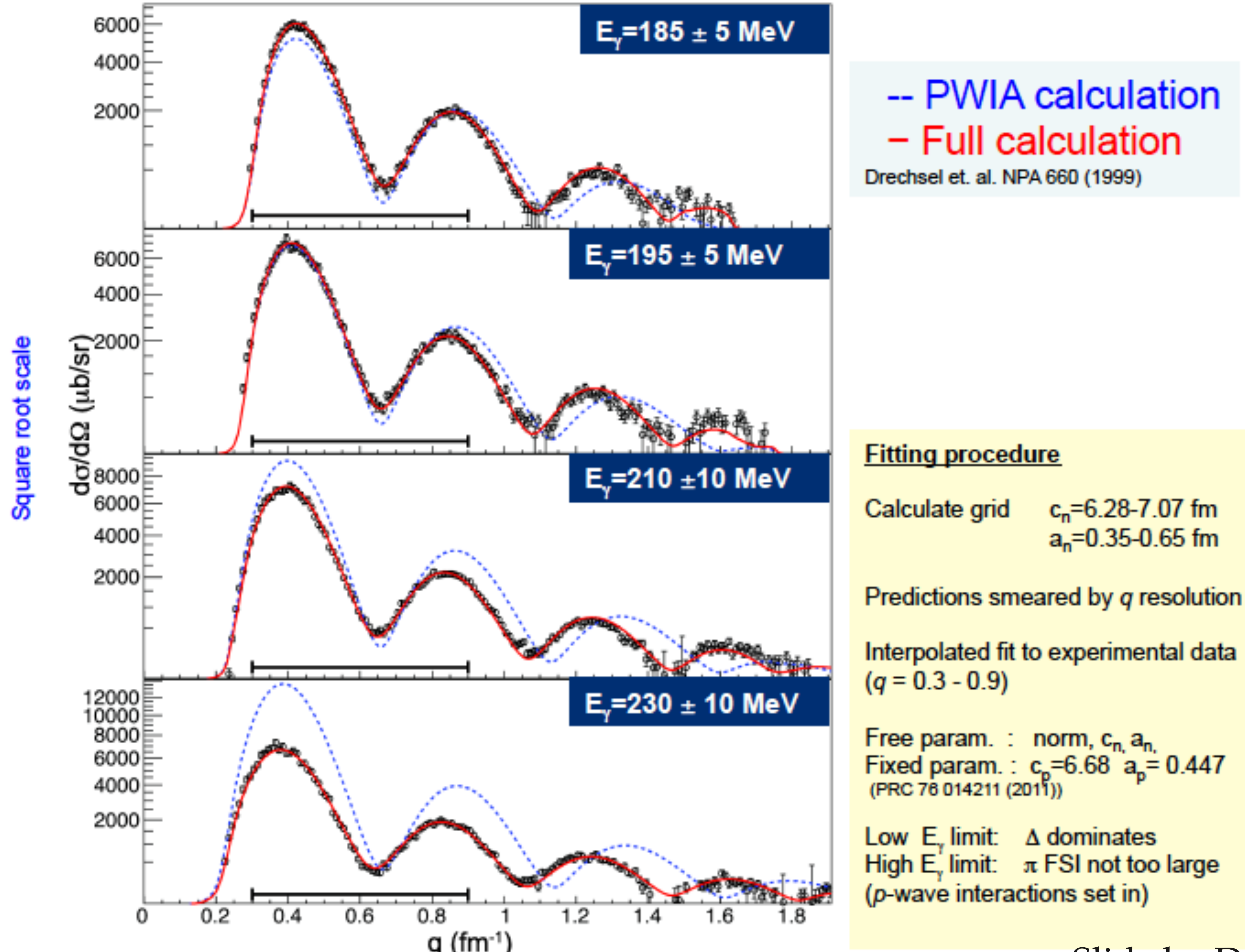

Fitting procedure

Calculate grid c_n=6.28-7.07 fm
a_n=0.35-0.65 fm

Predictions smeared by *q* resolution

Interpolated fit to experimental data
(*q* = 0.3 - 0.9)

Free param. : norm, c_n, a_n,
Fixed param. : c_p=6.68 a_p= 0.447
(PRC 76 014211 (2011))

Low E_γ limit: Δ dominates
High E_γ limit: π FSI not too large
(*p*-wave interactions set in)

Slide by D.P. Watts

Analysis

pion photo-production on a nucleon

[42] D. Drechsel, et al., NPA645, 145 (1999).

Unitary Isobar Model

We have developed a new operator for pion photo- and electroproduction for applications to reactions on nuclei at photon equivalent energies up to 1 GeV. The model contains Born terms, vector mesons and nucleon resonances up to the third resonance region ($P_{33}(1232)$, $P_{11}(1440)$, $D_{13}(1520)$, $S_{11}(1535)$, $F_{15}(1680)$, and $D_{33}(1700)$).

For the Born terms we propose an energy dependent superposition of pseudovector and pseudoscalar πNN couplings. This procedure describes the correct energy dependence of the non-resonant multipoles for photon *lab* energies up to $E_\gamma = 1$ GeV, in particular

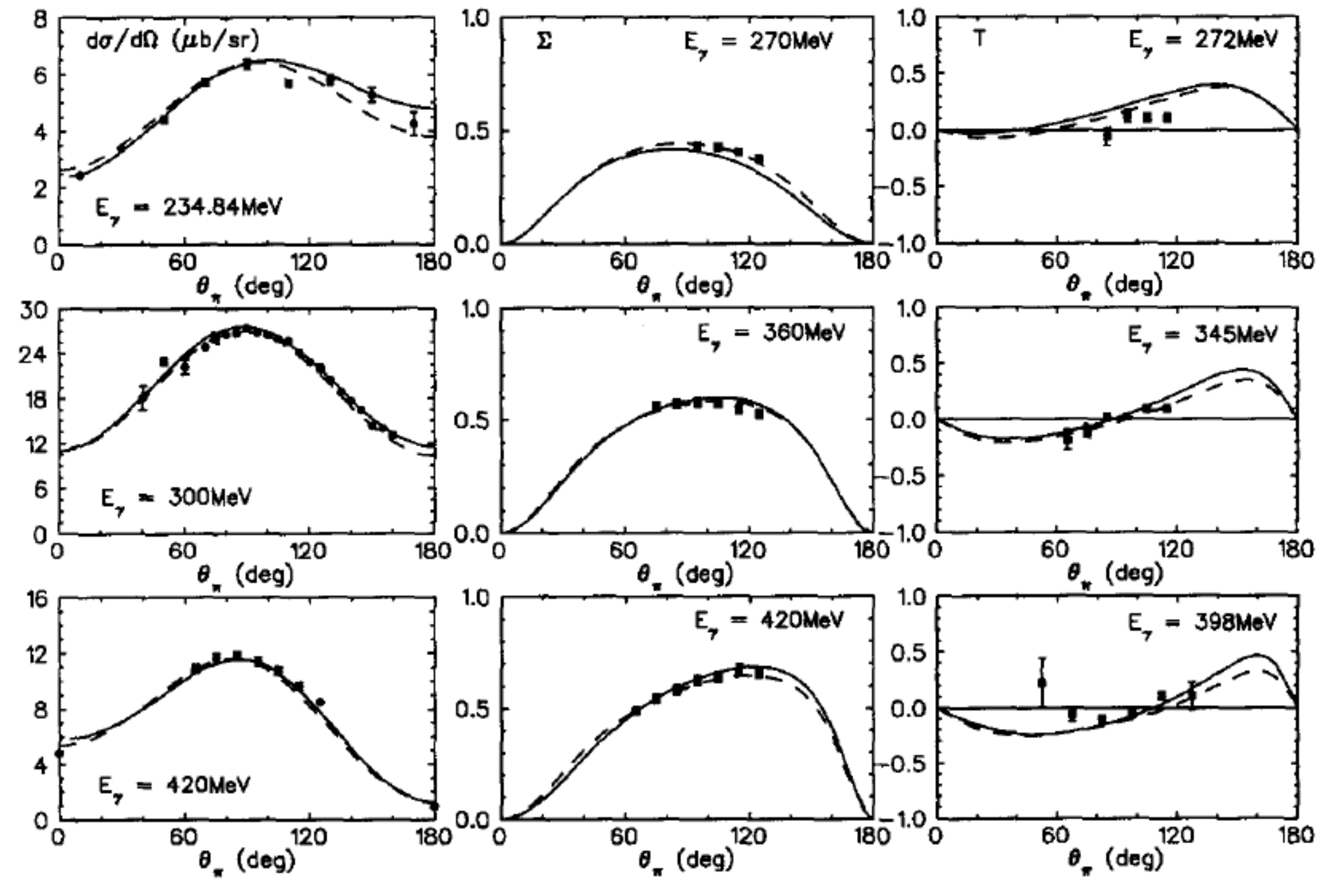

Fig. 8. The same as in Fig. 7 for $p(\gamma, \pi^0)p$. Experimental data from Refs. [28,29].

Analysis

pion nucleus optical potential

[42] D. Drechsel, et al., NPA645, 145 (1999).

A first-plus-second-order pion-nucleus optical potential constructed by fitting the phenomenological ϱ^2-dependent term to the π^{+-} - ^{12}C total and differential cross sections

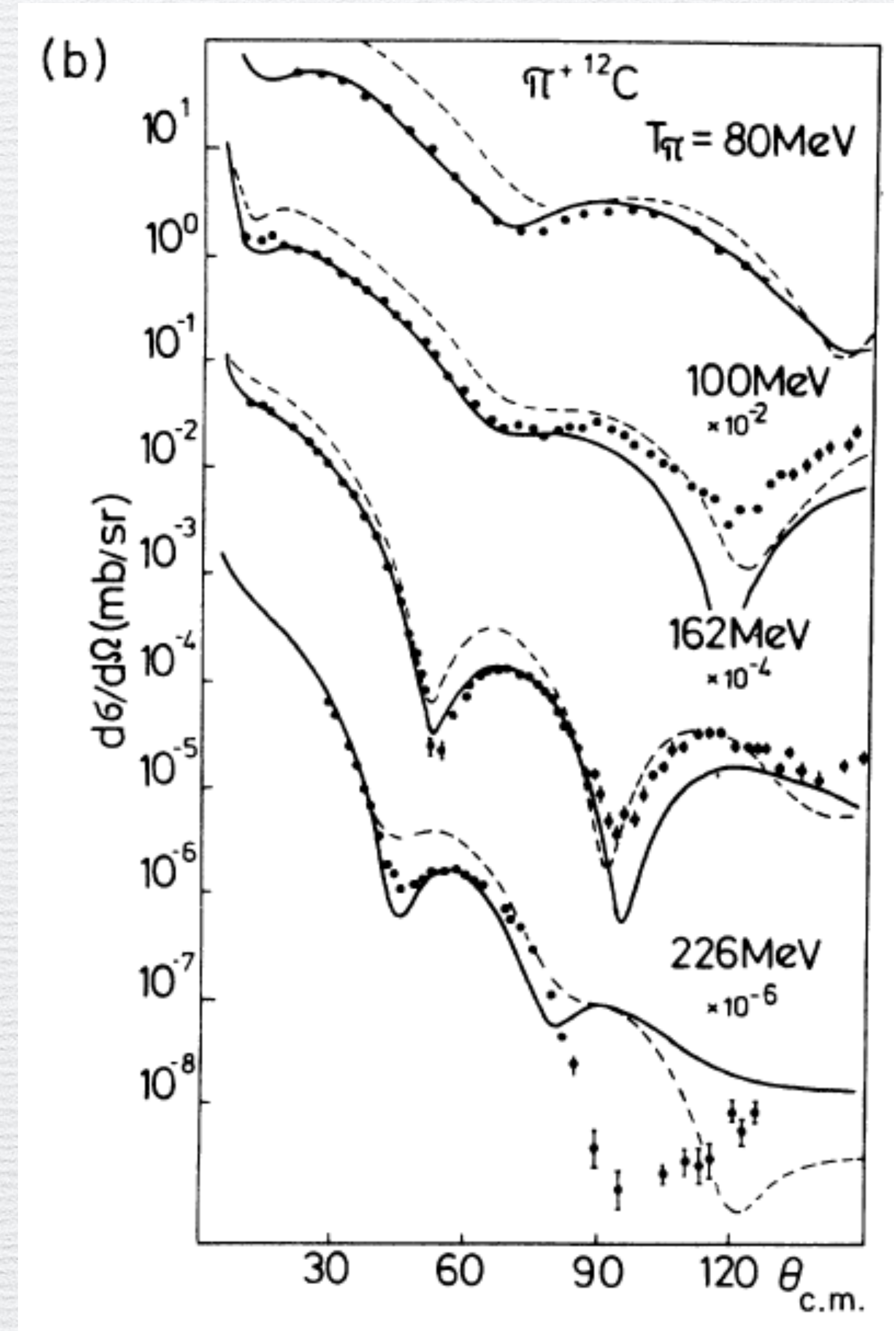

FIG. 2. Comparsion of theoretical calculations with the data for π scattering from ^{12}C. The dashed curves represent the results for $V^{(1)}$ and the solid curves include the effects of $V^{(2)}$ with B_0 and C_0 taken from Table I, while the dashed–double-dotted line is obtained with $V^{(2)}$ calculated for mesoatomic values (Ref. 19) $B_0=-0.043(1-i)$ and $C_0=-0.10(1-i)$. Data are from the following references: (a) $T_\pi=14$ MeV (Ref. 22), 20 MeV (Ref. 23), 30 MeV (Ref. 24; Ref. 26), 40 MeV (Ref. 25), 50 MeV (Ref. 24), 65 MeV (Ref. 28), 67.5 MeV (Ref. 27); (b) $T_\pi=80$ MeV (Ref. 28), 100 MeV (Ref. 29), 162 and 226 MeV (Ref. 30); (c) $120\leq T_\pi\leq 200$ MeV (Ref. 31), 226 MeV (Ref. 30; Ref. 31).

Analysis

pion photo-production on nuclei

[43] B. Krusche et al., PLB526, 287(2002)

Self-energy term in the Δ propagation fitted to to the ^{4}He data.

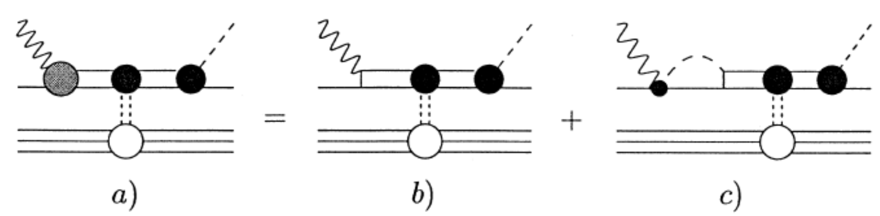

Fig. 1. Two main mechanisms of the Δ isobar excitation and corresponding medium effects: (b) direct excitation with the bare $\gamma N \Delta$ vertex; (c) vertex renormalization mechanism where the Δ isobar is excited from pions produced by non-resonant background.

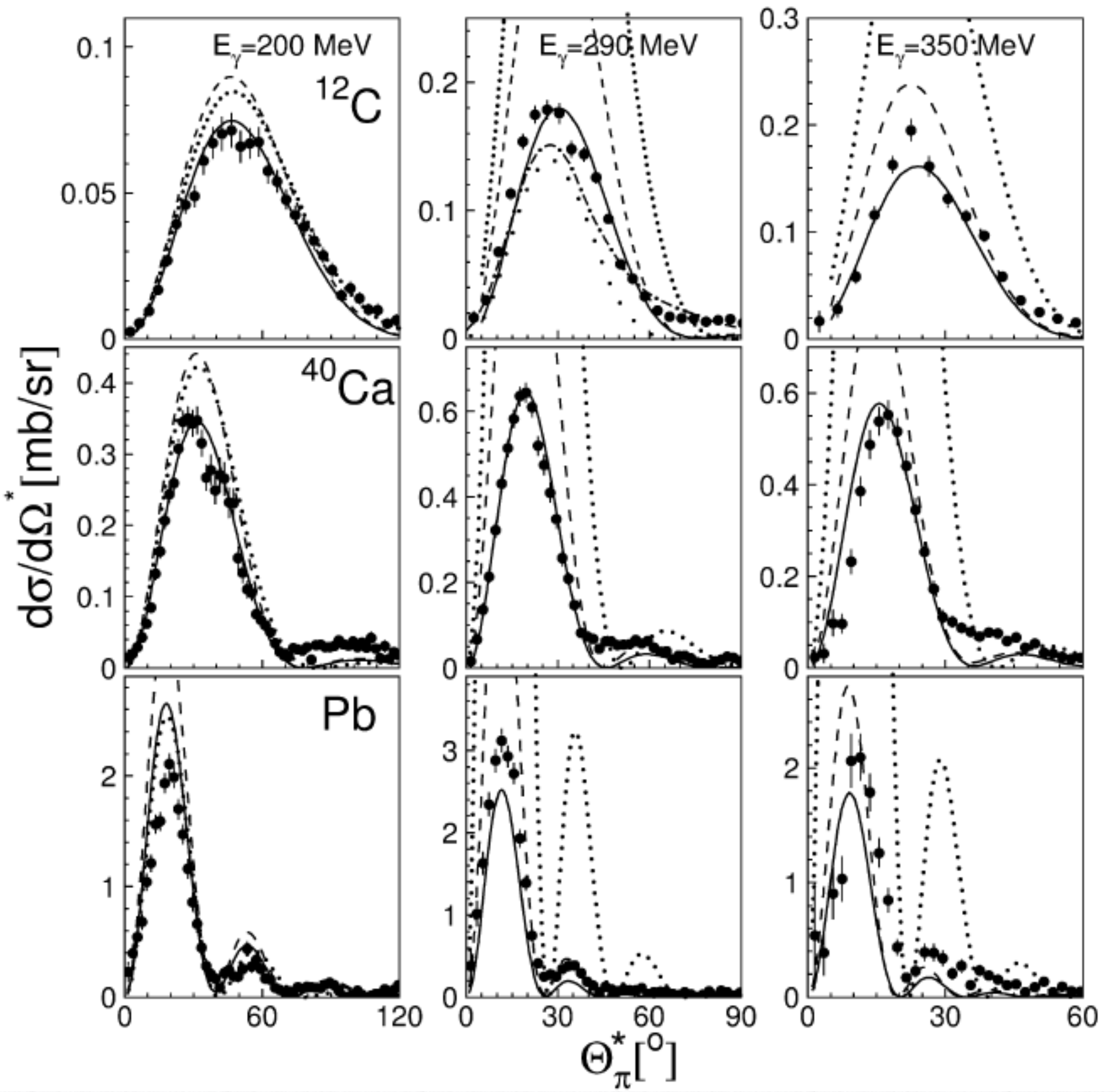

Fig. 4. Differential cross sections for $^{12}C(\gamma,\pi^0)^{12}C$, $^{40}Ca(\gamma,\pi^0)^{40}Ca$, and $Pb(\gamma,\pi^0)Pb$ compared to the predictions from Drechsel et al. [15]. Dotted lines: PWIA, dashed lines: DWIA, full lines: DWIA with Δ-self energy fitted to ^{4}He cross sections. For the carbon data at 290 MeV the predictions from Ref. [13] for the coherent reaction (wide space dotted) and coherent plus incoherent excitation of low lying states (dash-dotted) are also shown.

Analysis

Density Distribution

$\rho_p(r)$ [45]

$c_p = 6.680$ fm $a_p = 0.447$ fm

→ converted to point charge distribution incorporating the proton finite size

$\rho_n(r)$

calculated in the 35 grids ranging

$c_p = 6.28 - 7.07$ fm $a_p = 0.35 - 0.65$ fm

$$\rho(r) = \frac{Z}{A}\rho_p(r) + \frac{N}{A}\rho_n(r)$$

fitted with a **single 2PF distribution**

→ DWIA calculation

two parameter Fermi (2PF) distribution

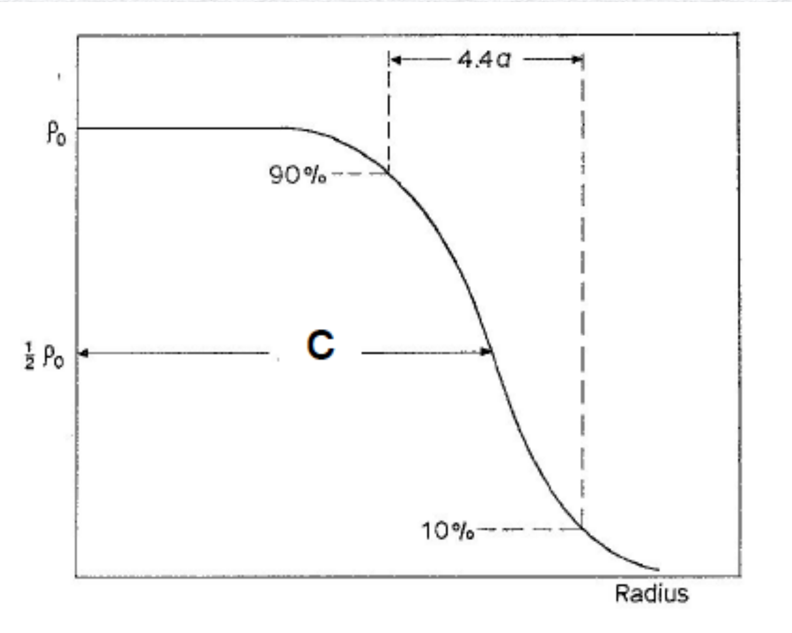

$$\rho(r) = \frac{\rho_0}{1 + \exp\left(\frac{r-c}{a}\right)}$$

smeared with experimental q resolution of 0.02-0.03 fm^{-1},
3% error is added to the c.s. data

Fitted to the data in q=0.3-0.9.
Interpolated in the ρ_n grids.

- discrepancy at high-q, probably due to inability of 2PF for describing the details of the density distribution
- discrepancy at high-E, probably due to the rapid increase of the π^0 absorption c.s. in the Δ resonance energy

Analysis

[44] To check the validity of approximating $\rho(r)$ by a single 2PF distribution, the Fourier transforms of $\rho(r)$ and the fitted 2PF distribution were compared. In the momentum range up to $q = 0.9\ \mathrm{fm}^{-1}$, over which the (γ, π^0) cross section was fitted to extract information about $\rho_n(r)$, the fractional difference between the two transforms only rises to 0.3% at $q = 0.9\ \mathrm{fm}^{-1}$.

Analysis

Momentum transfer distributions

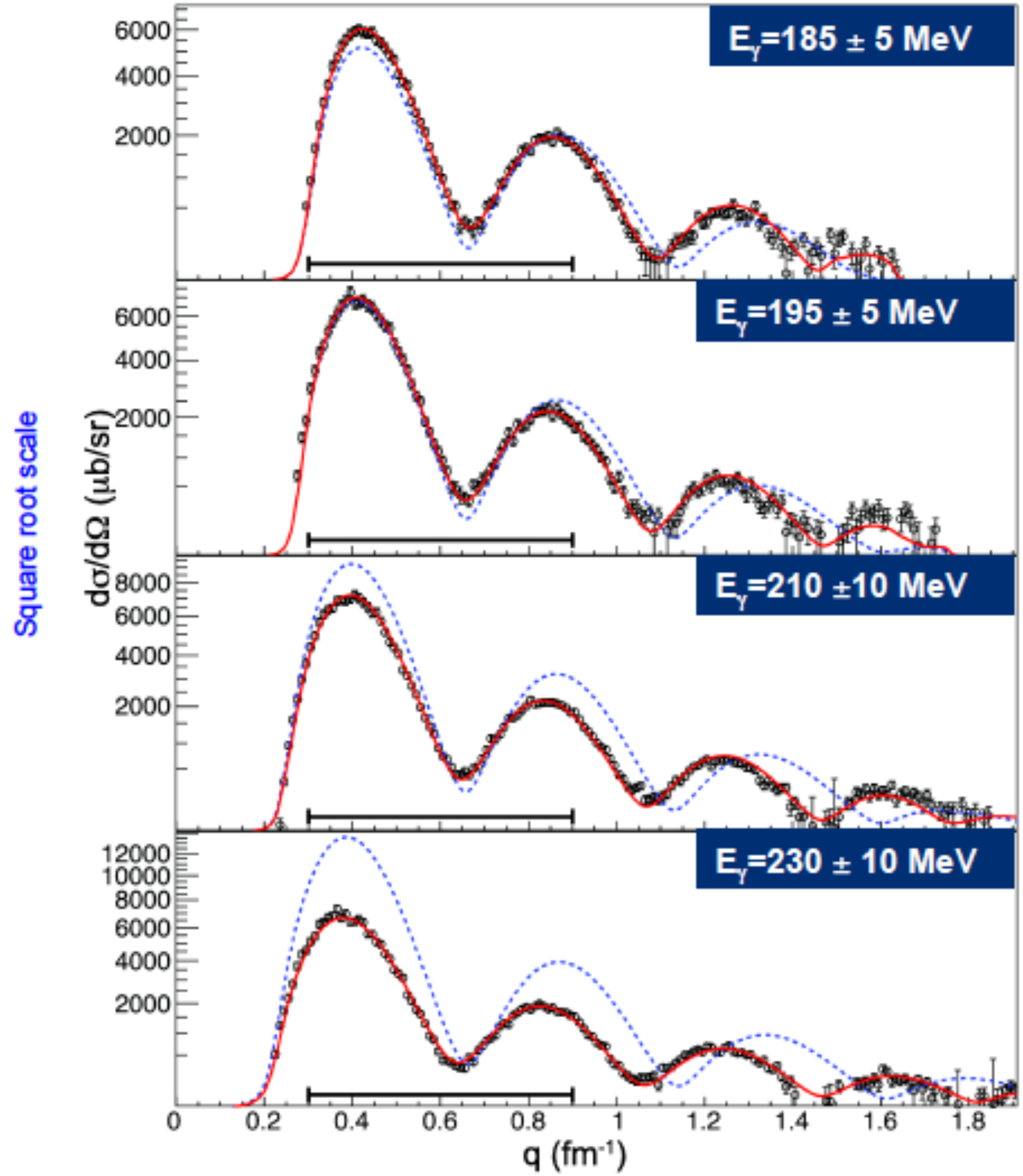

-- PWIA calculation
– Full calculation
Drechsel et. al. NPA 660 (1999)

Fitting procedure

Calculate grid c_n=6.28-7.07 fm
a_n=0.35-0.65 fm

Predictions smeared by *q* resolution

Interpolated fit to experimental data
(*q* = 0.3 - 0.9)

Free param. : norm, c_n, a_n,
Fixed param. : c_p=6.68 a_p= 0.447
(PRC 76 014211 (2011))

Low E_γ limit: Δ dominates
High E_γ limit: π FSI not too large
(*p*-wave interactions set in)

Slide by D.P. Watts

Results

The extracted skin properties

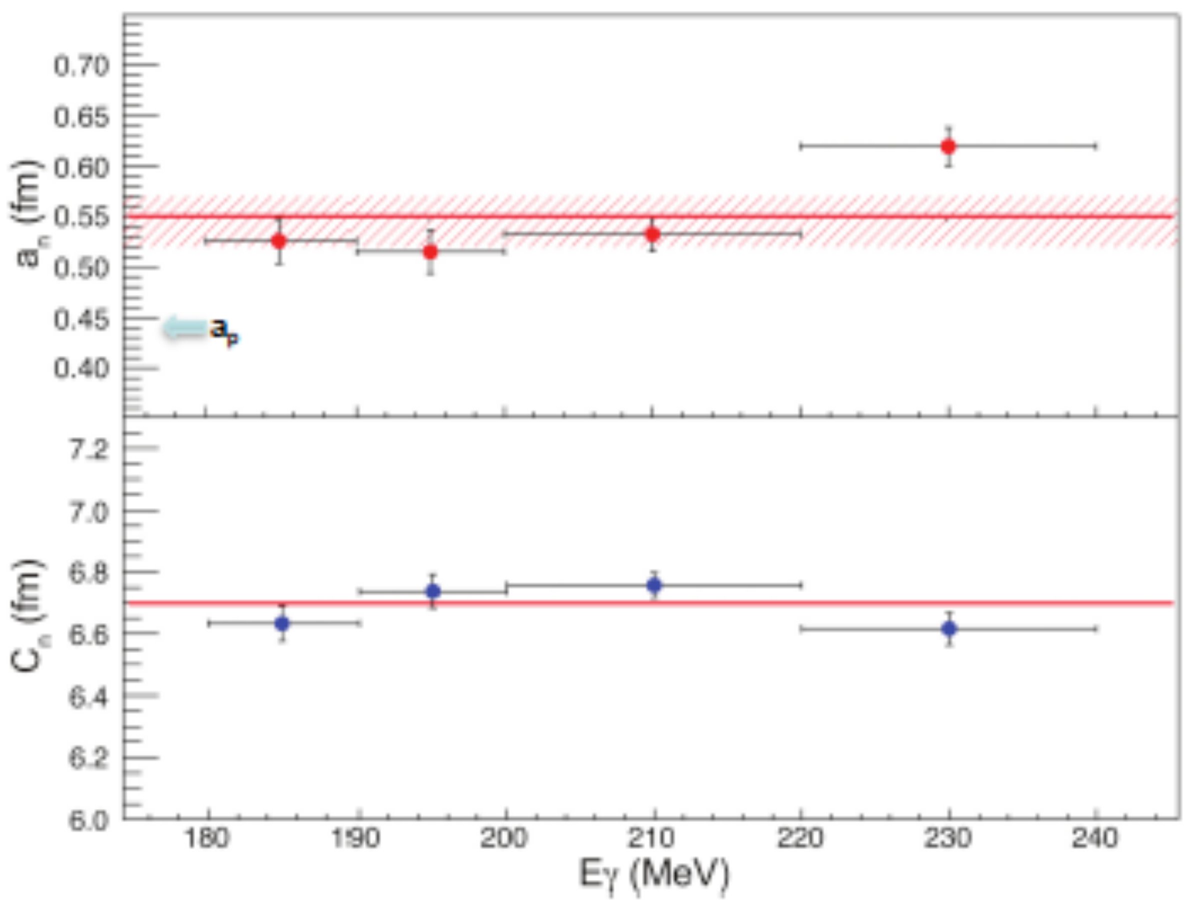

$$a_n = 0.55 \pm 0.01(stat.)^{+0.02}_{-0.03}(sys.)$$

$$c_n = 6.70 \pm 0.03(stat.)\mathrm{fm}$$

$$\Delta r_{np} = 0.15 \pm 0.03(stat.)^{+0.01}_{-0.03}(sys.)$$

- Systematics:
  - i) Normalisation parameter within ±5% of unity for all bins
  - i) E_γ dependences – a_n high E_γ bin 3.5σ away from average
  - ii) Vary yield fitting procedure
  - iii) 10% variation relative p,n amplitudes in the model (mainly affects diffuseness)
  - iv) Different fit ranges

Slide by D.P. Watts

Results

Systematic Error

- Analysis using only the first minimum
  → consistent result in the half-height radius ←How consistent?
- Variation of the relative weighting of the p and n amplitudes by 10%
  → change of 0.02 fm in the diffuseness and negligible effect on the half-height radius
- Variation in the modeling of the background
  → systematic error of 0.01 fm in the diffuseness ←How is the error in radius?

How is error in the reaction model?

Results

Half-height radius: **6.70±0.03(stat.)** fm ←How is the systematic error? Isn't the fluctuation in Fig.3 much larger?

Diffuseness: **0.55±0.01(stat.)+0.02-0.03(sys.)** fm

→ Δr_{np} = **0.15±0.03(stat.)+0.01-0.03(sys.)** fm

Results

Comparison with previous measurements

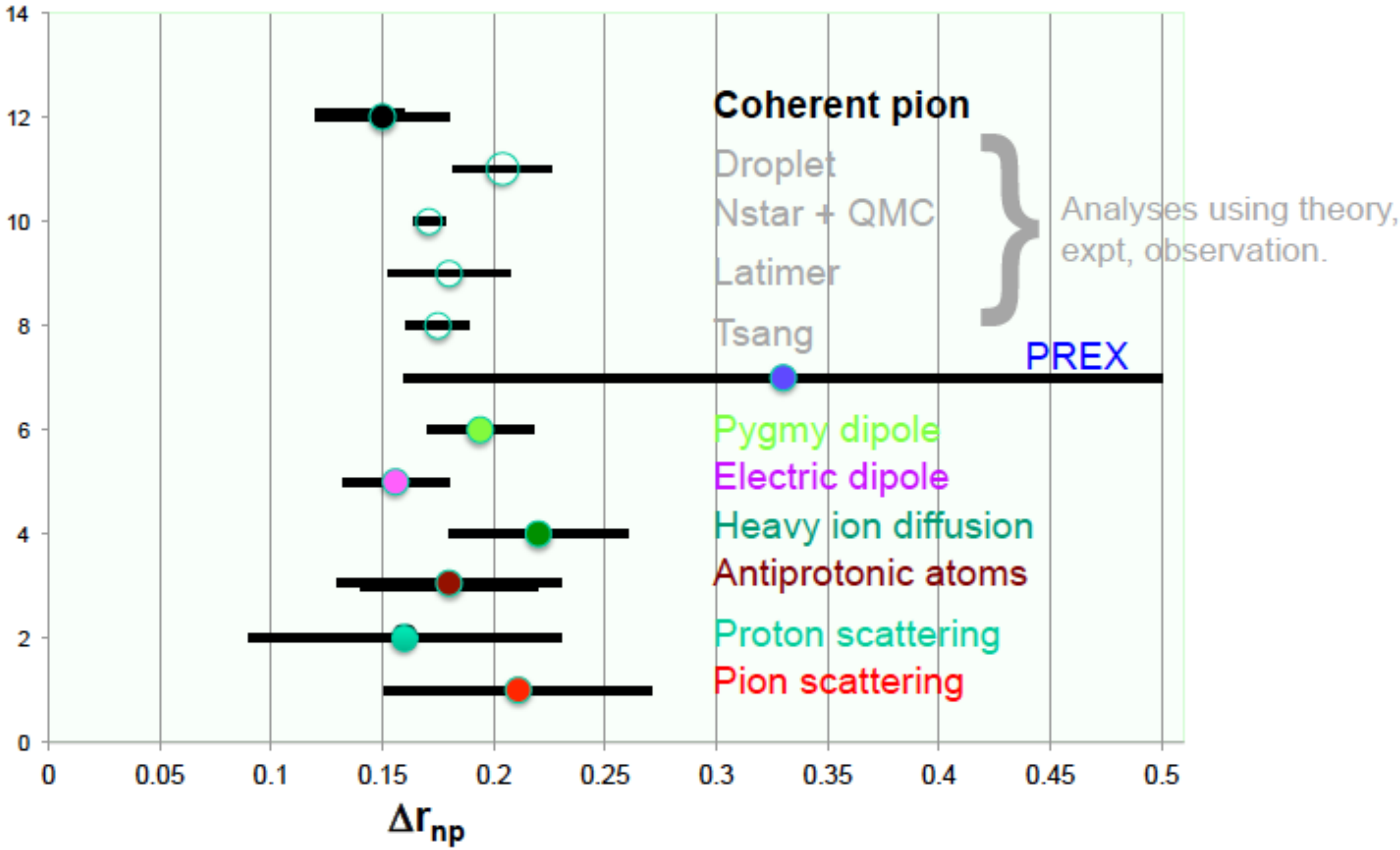

- New result in general agreement with other methods

Slide by D.P. Watts

Discussions

Comparison with theory

Slide by D.P. Watts

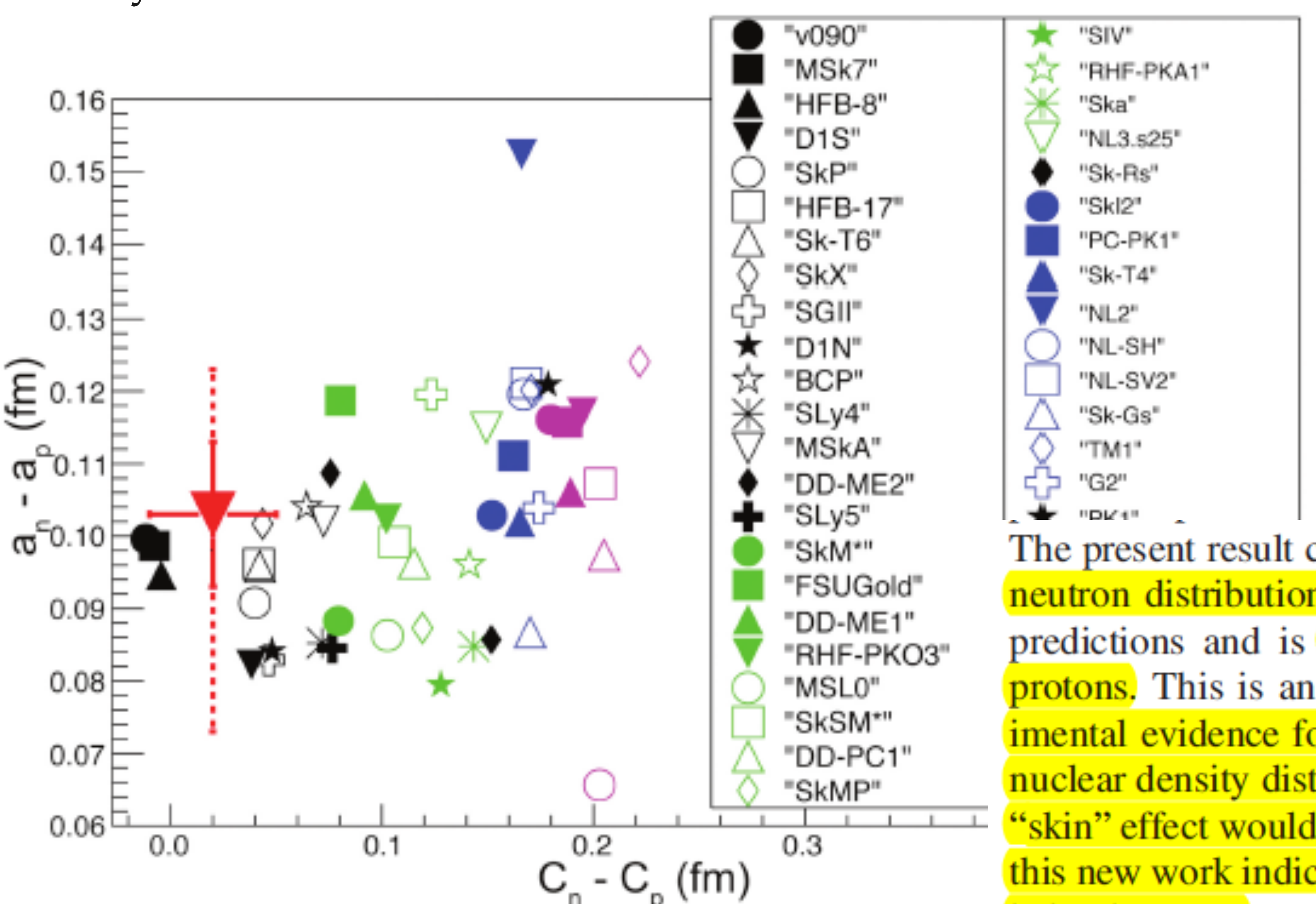

The present result clearly shows that the diffuseness of the neutron distribution in ^{208}Pb is in the range of theoretical predictions and is significantly greater than that for the protons. This is an important result, as conclusive experimental evidence for a difference in the diffuseness of the nuclear density distributions has been lacking [48]. A pure "skin" effect would have an $a_n - a_p$ value close to zero, so this new work indicates that the neutron skin of ^{208}Pb has a halo character.

Conclusive evidence that the neutron diffuseness is larger than the proton diffuseness → Halo?

Critical Discussions

- Why only at 180-240 MeV?
- Why only at q=0.3-0.9 fm^{-1}?
- How large is the model dependence of π^0-nucleus interaction?
- How is the assumption of the "single" two parameter Ferm distribution good enough?
- Pion charge-exchange contribution?
- Medium modification of the delta resonance? Pion production on the multiple nucleons?
- Uncertainty of the optical potential and pion propagation in medium?

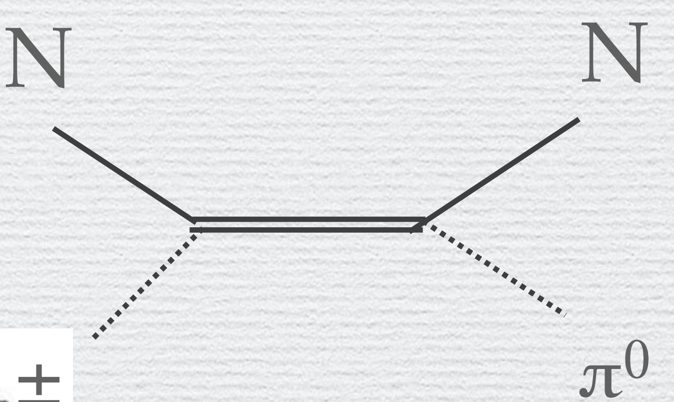

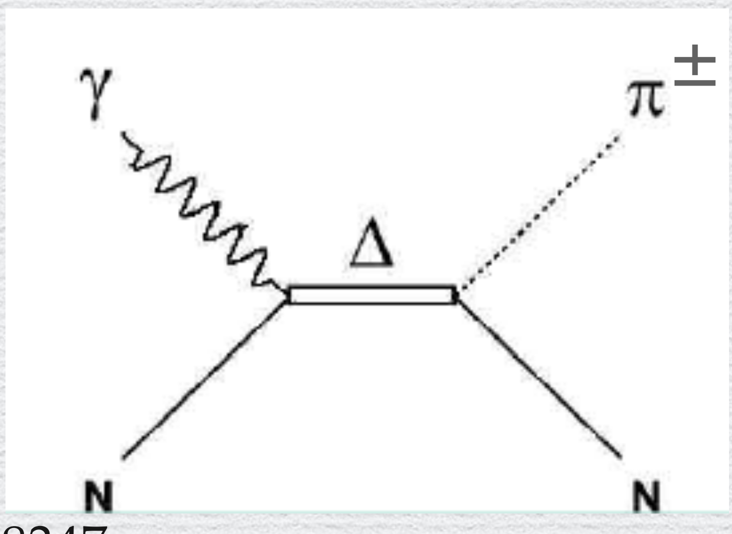

See also A. Gardestig , C.J. Horowitz, et al., arXiv:1504.08347

Discussions

Future plans

- Data under analysis for ^{116}Sn, ^{120}Sn, ^{124}Sn & ^{56}Ni
- Plans for ^{48}Ca, ^{40}Ca in future
- Discussions on Xenon isotopic chain

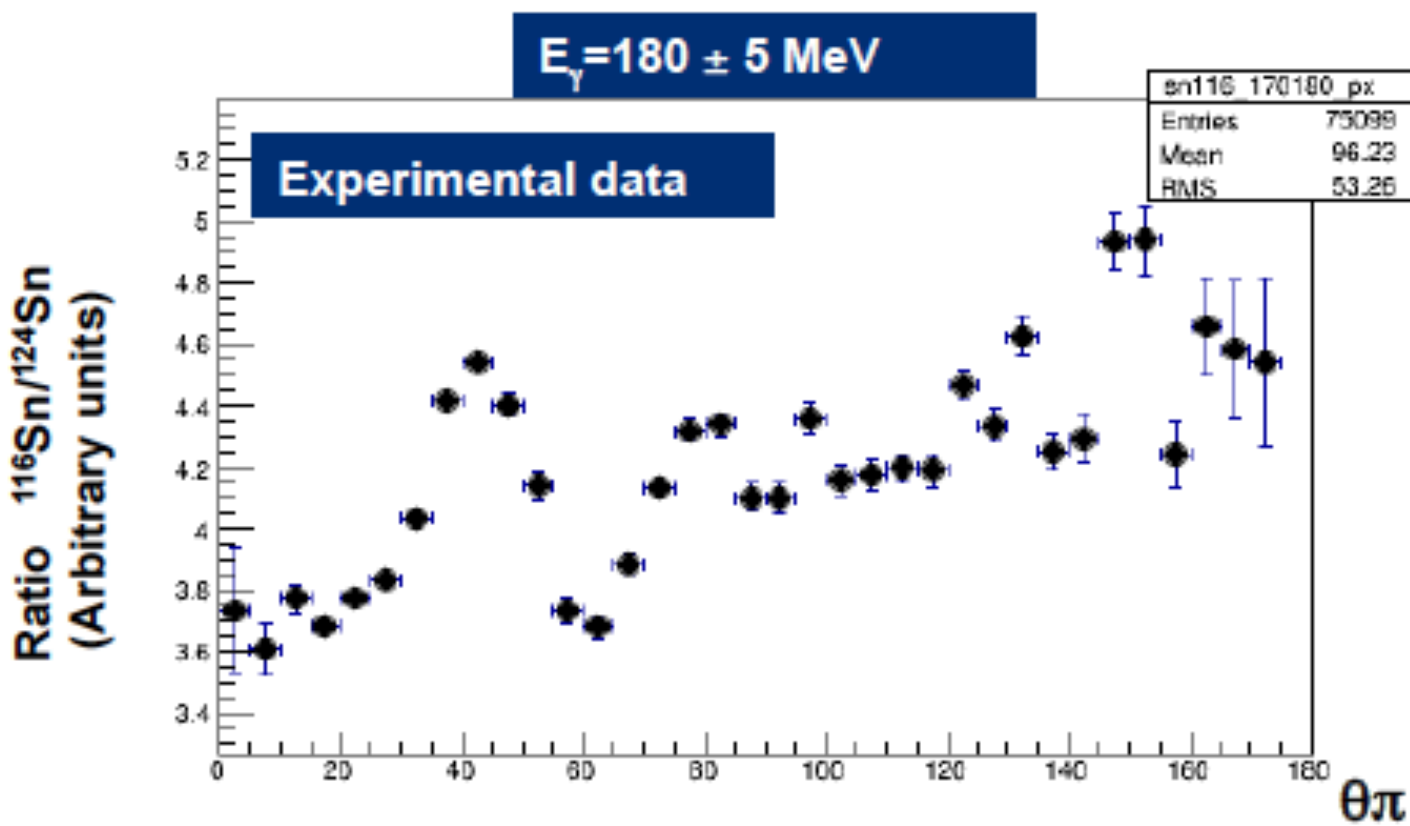

- Very early stage analysis

Slide by D.P. Watts

Summary

In summary, a measurement of the coherent photo-production of π^0 mesons from ^{208}Pb has provided the first determination of a nuclear matter form factor with an electromagnetic probe. The existence of a neutron skin on the surface of the ^{208}Pb nucleus is confirmed with a thickness $\Delta r_{np} = 0.15 \pm 0.03(\text{stat.})^{+0.01}_{-0.03}(\text{sys.})$ fm. The method is sensitive enough to extract the shape of the neutron distribution, which is found to be ~20% more diffuse than the charge distribution. This new determination of the neutron skin properties discriminates against some of the modern nuclear theories in common use and will be a valuable new constraint on the equation of state for neutron-rich matter and neutron stars.